END
DATE
FILMED

DTIC

MICROCOPY RESOLUTION TEST CHART
NATIONAL BUREAU OF STANDARDS-1963-A

AFWAL-TR-82-3018

AD A127950

WIND TUNNEL EXPERIMENTS ON THE DIVERGENCE
OF SWEPT WINGS WITH COMPOSITE STRUCTURES

Maxwell Blair
Analysis and Optimization Branch
Structures and Dynamics Division

October 1982

Final Technical Report for the Period June 1979 – June 1981

83 05 12 015

FLIGHT DYNAMICS LABORATORY
AIR FORCE WRIGHT AERONAUTICAL LABORATORIES
AIR FORCE SYSTEMS COMMAND
WRIGHT-PATTERSON AIR FORCE BASE, OHIO 45433

This technical report has been reviewed and is approved for publication.

MAXWELL BLAIR
Project Engineer
Aeroelastic Group
Analysis & Optimization Branch

FREDERICK A. PICCHIONI, Lt Col, USAF
Chief, Analysis & Optimization Branch
Structures & Dynamics Division

FOR THE COMMANDER

RALPH L. KUSTER, Col, USAF
Structures & Dynamics Division

REPORT DOCUMENTATION PAGE		READ INSTRUCTIONS BEFORE COMPLETING FORM
1. REPORT NUMBER AFWAL-TR-82-3018	2. GOVT ACCESSION NO. AD. A127950	3. RECIPIENT'S CATALOG NUMBER
4. TITLE (and Subtitle) WIND TUNNEL EXPERIMENTS ON THE DIVERGENCE OF SWEPT WINGS WITH COMPOSITE STRUCTURES		5. TYPE OF REPORT & PERIOD COVERED Final Report
		6. PERFORMING ORG. REPORT NUMBER
7. AUTHOR(s) Maxwell Blair		8. CONTRACT OR GRANT NUMBER(s)
9. PERFORMING ORGANIZATION NAME AND ADDRESS Analysis and Optimization Branch Flight Dynamics Laboratory Air Force Wright Aeronautical Laboratories Wright-Patterson AFB, Ohio 45433		10. PROGRAM ELEMENT, PROJECT, TASK AREA & WORK UNIT NUMBERS Project 2401 Task 240102 Work Unit 24010239
11. CONTROLLING OFFICE NAME AND ADDRESS Air Force Wright Aeronautical Laboratories Air Force Systems Command Wright-Patterson AFB, Ohio 45433		12. REPORT DATE October 1982
		13. NUMBER OF PAGES 77
14. MONITORING AGENCY NAME & ADDRESS(if different from Controlling Office)		15. SECURITY CLASS. (of this report) Unclassified
		15a. DECLASSIFICATION/DOWNGRADING SCHEDULE

16. DISTRIBUTION STATEMENT (of this Report)

Approved for public release; distribution unlimited.

17. DISTRIBUTION STATEMENT (of the abstract entered in Block 20, if different from Report)

18. SUPPLEMENTARY NOTES

19. KEY WORDS (Continue on reverse side if necessary and identify by block number)

Aeroelasticity
Composites
Forward Swept Wing
Wind Tunnel Test
Divergence

20. ABSTRACT (Continue on reverse side if necessary and identify by block number)

An elastic wing with variable sweep was designed and subcritically tested for aeroelastic divergence in the Virginia Tech six foot stability wind tunnel. This wing has an internal interchangeable graphite/epoxy plate that provides the wing stiffness. This plate had the shape of a high aspect ratio trapezoid with a line of symmetry coincident with the spanwise wing reference axis. A fiberglass aerodynamic shell with ten chordwise sections surrounds the plate. These shell sections were mounted so as to minimize their stiffness contribution →

DD FORM 1473 EDITION OF 1 NOV 65 IS OBSOLETE
1 JAN 73

to the plate and still maintain good aerodynamic performance. A series of six symmetric plates with various fiber orientations were constructed. Fiber layup on each plate is symmetric about the midplane parallel to the surface. By inverting the plate, it was possible to test 11 unique fiber orientations. Theoretically, identified test results predicted relationships between wing sweep, fiber orientation, and divergence speed. One configuration, tested to the divergence speed, showed good correlation with the subcritically projected divergence speed.

Maximum divergence speed was found to occur for wings with fibers swept 0 to 30 degrees forward of the spanwise reference axis. Minimum divergence speed was found for wings with fibers swept aft of the spanwise reference axis.

FOREWORD

AFWAL-TR-82-3018

TABLE OF CONTENTS

LIST OF ILLUSTRATIONS

LIST OF ILLUSTRATIONS (CONT'D)

LIST OF SYMBOLS

SYMBOL:

c	structural chord
e	elastic axis offset, the distance between the aerodynamic center and the elastic axis (pitch axis on two-dimensional airfoil), measured positive with aerodynamic center in front of elastic axis
EI	bending stiffness
GJ	torsional stiffness
k	rotational spring stiffness
M	bending moment on a beam
M_e	elastic (structural) restoring moment
M_a	aerodynamic moment
q	free stream dynamic pressure
q_d	free stream dynamic pressure at divergence
S	planform area of wing
T	torque on a beam
X	dimension of beam length
$\dfrac{dC_L}{d\alpha}$	lift curve slope
α	angle-of-attack measured away from the zero lift angle-of-attack
α_o	zero airspeed angle-of-attack
α_r	wing root angle-of-attack
ϵ	strain
Λ	wing sweep measured positive aft and zeroed when the reference axis is perpendicular to the free stream velocity (see Figure 15)
θ	fiber orientation measured counter clockwise from the structural chordwise direction which is perpendicular to the reference axis
σ	bending deformation angle
ϕ	twisting deformation angle

SECTION I

INTRODUCTION

Substantial effort has been directed toward the goal of producing low cost, high performance aircraft. Since Krone presented his work with material tailoring to the AIAA in 1975 (Reference 1), forward swept wing application on advanced fighters has been investigated. Subsequent analysis has shown the potential for aircraft weight reduction and fiscal savings while meeting anticipated future performance requirements (Reference 2). A forward swept wing technology base is now necessary to firmly establish this design as a widely accepted alternative.

Each of several corporate efforts has independently concentrated on their design of a baseline configuration (Reference 3). These proposed configurations answer a need for a prototype demonstrator in the early 1980's. Whereas the need for a demonstrator has been presented (Reference 3), emphasis also needs to be given toward research which provides a comprehensive view of forward swept wing technology. This research could be used in conjunction with flight demonstrator data to enhance the design engineer's understanding of forward swept wing design. For instance, the current report presents experimental results which relate wing sweep and fiber orientation to clamped wing divergence speeds. Other research may be directed to establish the relationship between mass distribution and dynamic characteristics of a free-free forward swept wing aircraft. The list of research requirements which relate to forward swept wing technology is not limited to these two examples.

Since the inception of swept wing designs, only wing divergence has withheld the forward sweep alternative from consideration. As a result of German wartime tests with forward swept wings, Convair began design studies in 1945 which proposed a fast attack bomber with 30 degrees of forward wing sweep (Reference 4). Before airframe construction was completed, the development program was cancelled. Reasons for cancellation were not given in the account of Reference 4. In 1948, Diederich

and Budiansky showed that forward sweep of metallic wings lowered the clamped wing divergence speed (Reference 5). A comprehensive view of this divergence problem is given by Bisplinghoff, Ashley, and Halfman (Reference 6).

During the 1960's, advanced composite materials were developed and much progress was made in fibrous laminate theory. During the same period of time, new high speed digital computers provided the capability to perform extensive analyses of laminated structure. With the use of optimization algorithms, Schmit (Reference 7) proposed a method of structural synthesis with composite materials. His was an early attempt to develop a method by which engineers could best exploit the directional properties of composites. It was a combination of materials technology and computer technology that gave birth to a new technology now known as aeroelastic tailoring. Aeroelastic tailoring is the application of composite materials for the purpose of aeroelastic optimization. Time and interest was directed toward this field by many people. In 1972, McCullers and Lynch presented a computer code for aeroelastic optimization with composite materials (Reference 8). Subsequent work in the field of aeroelastic optimization yielded results which promised substantial improvement in aircraft performance through weight savings and passive shape control (Reference 9).

In 1975, Krone proposed the application of composite materials to alleviate weight penalties which were associated with the divergence characteristic of forward swept wings (Reference 1). With the use of optimization technology provided by the Air Force Flight Dynamics Laboratory, Krone was able to present results of two wing configuration studies which showed that only small weight increases were required to avoid divergence when the swept forward design replaced the conventional aft swept design.

In 1979, both Rockwell International (Reference 10) and Grumman Aerospace (Reference 11) performed wind tunnel tests on their forward swept wing base-line configurations. The results provided experimental

proof that wing divergence could be alleviated for forward swept wings. However, these extensive tests did more to prove the individual designs than to contribute to a comprehensive understanding. Other wind tunnel experiments were presented by Sherrer, Hertz and Shirk (Reference 12) and Ricketts and Doggett (Reference 13). These projects developed new approaches to aeroelastic testing of forward swept wings. The data from these tests were the first contributions toward a broad data base which would verify aeroelastic tailoring principles for the prevention of divergence on forward swept wings. More specifically, Reference 12 provided a confirmation of analytic tools used in forward swept wing stability analysis. Reference 13 contains an excellent overview of experimental methods that directly pertain to the subject of this report.

Weisshaar (Reference 14) presented a portion of his DARPA and Air Force sponsored work in aeroelastic tailoring in 1980. This research was concurrent with efforts at the Air Force Flight Dynamics Laboratory and at NASA Langley. His efforts were directed toward theoretical development of the ground work laid by Krone. To do this, Weisshaar developed a segmented laminated beam analysis computer code which featured low cost and low computer time. With lifting line aerodynamics, his numerical results presented a new view of the relationship between fiber orientation, wing sweep, and clamped divergence speed.

In the left half of Figure 1 a forward swept wing is shown with all fibers in the spanwise direction. This wing has no structural bend/twist coupling and deformation is increased near the divergence speed as is typical of a forward swept conventional wing with conventional design with metallic structure. This type of wing which characteristically increases angle-of-attack under load is said to washin. Figure 1 also shows the same wing configuration with fibers swept forward of the spanwise axis. This wing is anisotropic with respect to the structural axis. The bend/twist coupling keeps the wing tip at a constant angle-of-attack, thus washin is neutralized. A wing which is designed to decrease angle-of-attack with increased bending is said to washout. By controlling washin on a forward swept wing design, it is possible to control static aeroelastic divergence.

3
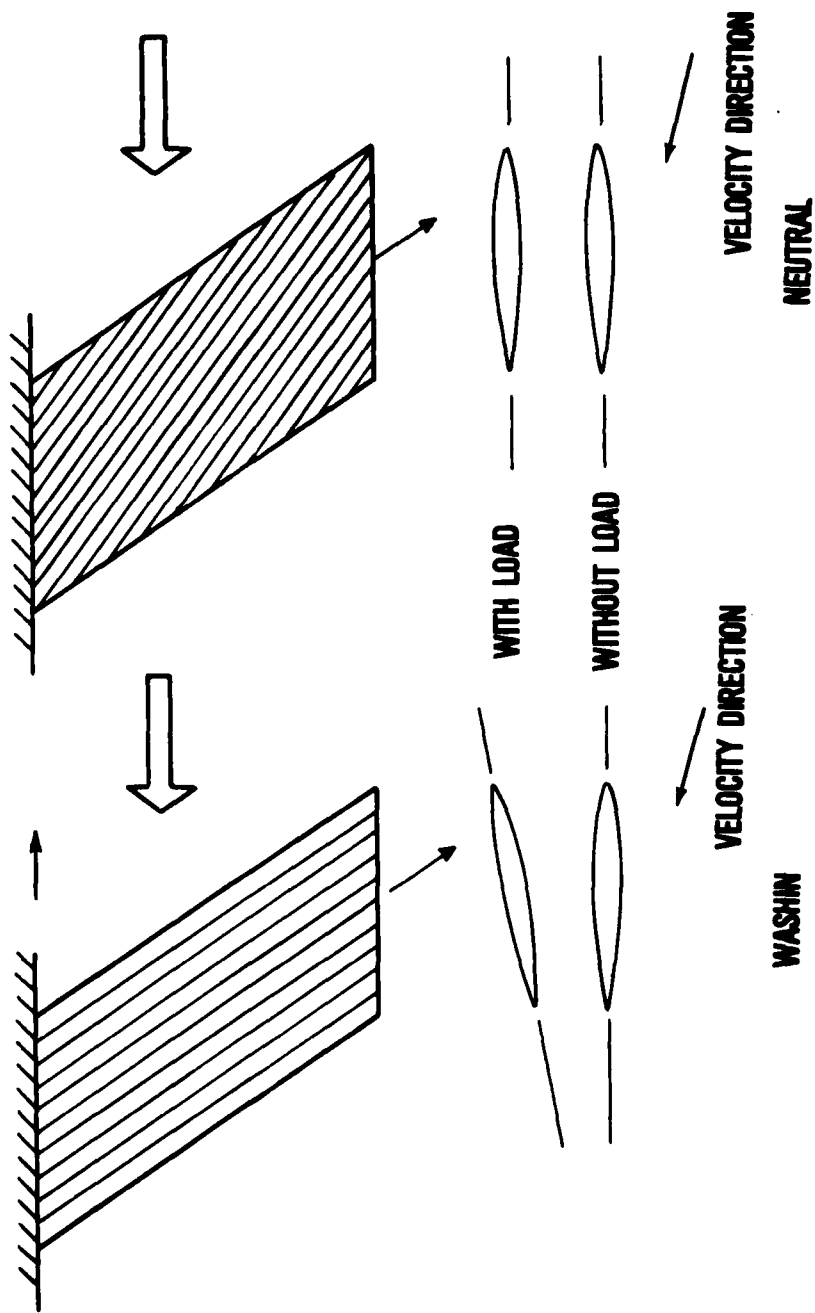
Figure 1. A General Relationship Between Fiber Orientation and Washin

While effort has been expended on analysis for aeroelastic tailoring of forward swept wings, there still remains a very small experimental data basis. This present report contains a theme very similar to Weisshaar's work, but on an experimental basis. Here, the need for a physical verification of aeroelastic tailoring techniques is recognized. Instead of confirming the validity of analytic methods, this set of experiments was designed to clearly demonstrate the fundamental relationships between fiber orientation, wing sweep, and wing divergence speed. This report presents an experimental exposition of aeroelastic tailoring for the prevention of wing divergence.

SECTION II

A REVIEW OF THE DIVERGENCE PHENOMENON

The shape of an object determines aerodynamic load. Aerodynamic load changes the shape of a flexible object. Static aeroelasticity is the exclusive study of the mutual interaction between steady aerodynamics and an elastic body. An anisotropic body has material properties that are directionally dependent. In the analysis of a wing with anisotropic behavior, coupling between bending and twisting becomes an important factor that may not be apparent in classical wing design. Bend/twist coupling may be utilized to prevent wing divergence, a static aeroelastic instability which is documented in Reference 6.

Wing divergence may be confused with static aeroelastic overloading. The distinction between the two is important to the understanding of static aeroelastic stability. For an aircraft in steady level flight, total wing load remains nearly constant at all subcritical velocities. For a conventionally designed metallic wing with forward sweep, the rate of wing loading with respect to angle-of-attack is amplified with increasing velocity. While this total wing loading remains a constant for undisturbed level flight near the divergence speeds, small perturbations in aircraft angle-of-attack result in large structural deformations. The divergence velocity is the speed at which infinitely large static deflections would result from infinitesimal perturbations in aircraft angle-of-attack.

Figure 2 shows a typical symmetric, two-dimensional airfoil with one rotational degree of freedom. The rotational spring, with stiffness k, provides a restoring moment in opposition to the aerodynamic load. This load is assumed to act on the airfoil at the aerodynamic center according to thin airfoil theory. The elastic restoring moment is

$$M_e = k(\alpha - \alpha_0). \tag{1}$$
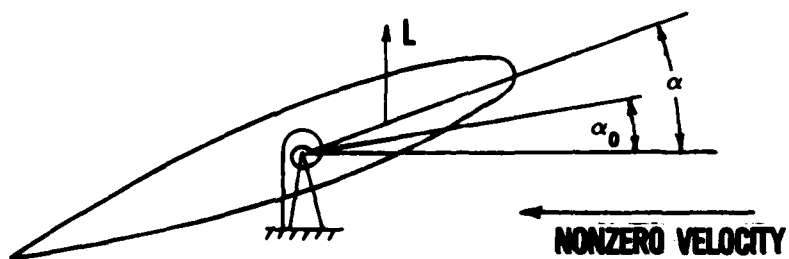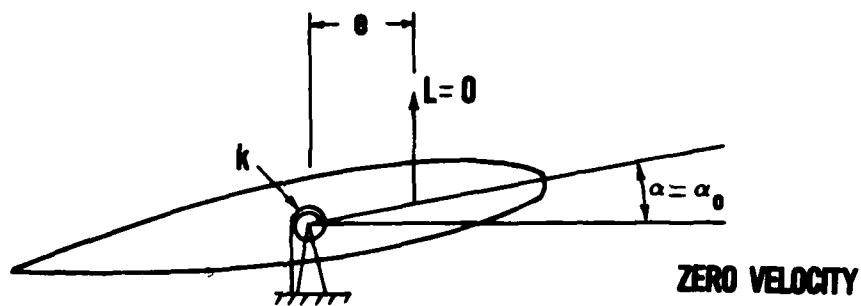
Figure 2.   Schematic of a Two-Dimensional Aeroelastic Airfoil

The aerodynamic moment at the center of rotation, representative of an elastic axis, is

$$M_a = -(\frac{dC_L}{d\alpha}) \, q \, Se\alpha \tag{2}$$

Equilibrium requires that the elastic restoring moment always be capable of resisting the imposed aerodynamic moment at the elastic axis. With algebraic operations, the following relation can be derived:

$$\alpha = \frac{\alpha_0}{1 - \dfrac{q}{q_d}} \tag{3}$$

where

$$q_d = \frac{k}{eS(\dfrac{dC_L}{d\alpha})} \tag{4}$$

As the free stream dynamic pressure, q, approaches q_d, the divergence dynamic pressure, the angle-of-attack, α, becomes very large. In terms of static aeroelastic response, infinite angles-of-attack are approached as the dynamic pressure reaches divergence conditions, even for small values of α_0 relative to the zero lift angle-of-attack. In Figure 3, the relationship between α and q is given for various values of constant α_0, the zero airspeed angle-of-attack.

More insight into the divergence phenomenon may be extracted by inspecting the aerodynamic moment at the elastic axis and the elastic restoring moment independently (Reference 6). For a small change in α, the aerodynmic moment at the elastic axis changes by

$$\Delta M_a = \frac{dC_L}{d\alpha} \, q \, Se\Delta\alpha \tag{5}$$
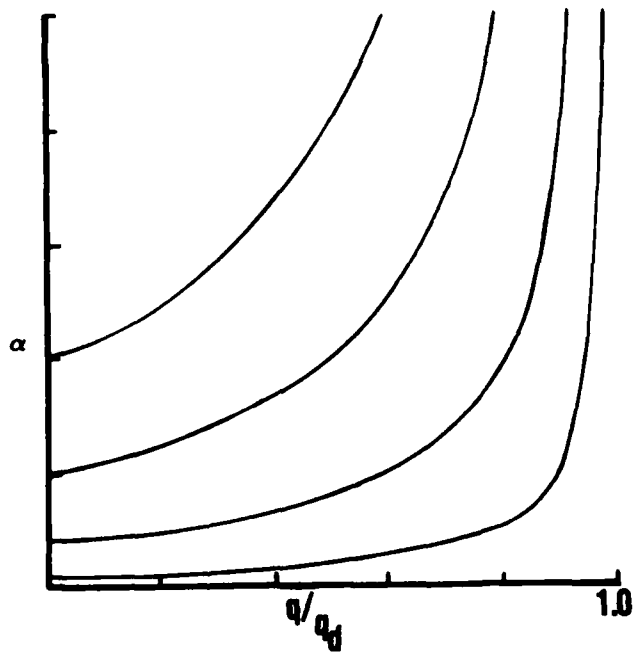
Figure 3.   Aeroelastic Relationship Between Angle-of-Attack and
Normalized Dynamic Pressure

and the elastic restoring moment changes by

$$\Delta M_e = k\Delta\alpha \qquad\qquad (6)$$

By plotting change in moment with respect to angle-of-attack, $\dfrac{\Delta M_e}{\Delta\alpha}$ and $\dfrac{\Delta M_\alpha}{\Delta\alpha}$ as a function of q in Figure 4, it is seen that the two lines cross when dynamic pressure reaches the divergence dynamic pressure.

The divergence q is reached when the elastic restoring moment can-not compensate for small changes in the aerodynamic load caused by per-turbations in angle-of-attack. One may interpret the quantity $(\Delta M_e - \Delta M_a)/\Delta\alpha$ as the overall potential to restore the wing to equilibrum. As shown in Figure 4, this quantity becomes small near the divergence speed. Physically, one should not be surprised to see the wing "float" about equilibrium when the overall restoration potential is lost near divergence conditions.

The principle of wing divergence of a two-dimensional section is readily extended to a conventional slender straight finite wing. Even though both wing bending and wing twist are present, the two deforma-tions are not coupled. Equations governing this phenomenon are presented in Reference 6. Wing sweep complicates the analysis substan-tially. The relationship between bending deformation and aerodynamic angle-of-attack couple the equilibrum equations which represent wing bending and wing twist.

In Figure 5, a forward swept wing is modeled by a forward swept paddle-like surface. A rotational spring with stiffness, k, gives this rigid surface restoring potential similar to bending stiffness. Flow is parallel to line BC when the wing is undeflected and when the wing deflects, parallel lines AB and CD remain parallel to the undeflected positions. In the undeflected state, the airflow is parallel to the surface and in line with points B and C. As the angle-of-attack and the load are increased, the wing deflects and consequently point B is raised relative to point C. The airflow encounters the wing surface at the root angle-of-attack plus a component of deflection angle-of-attack.
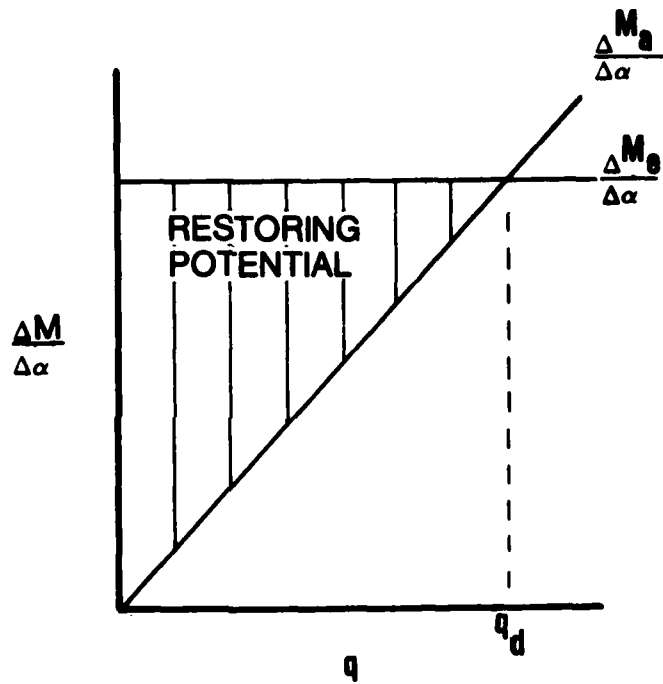
Figure 4.   Relationship   Between   Restoring   Potential   and   Dynamic
Pressure
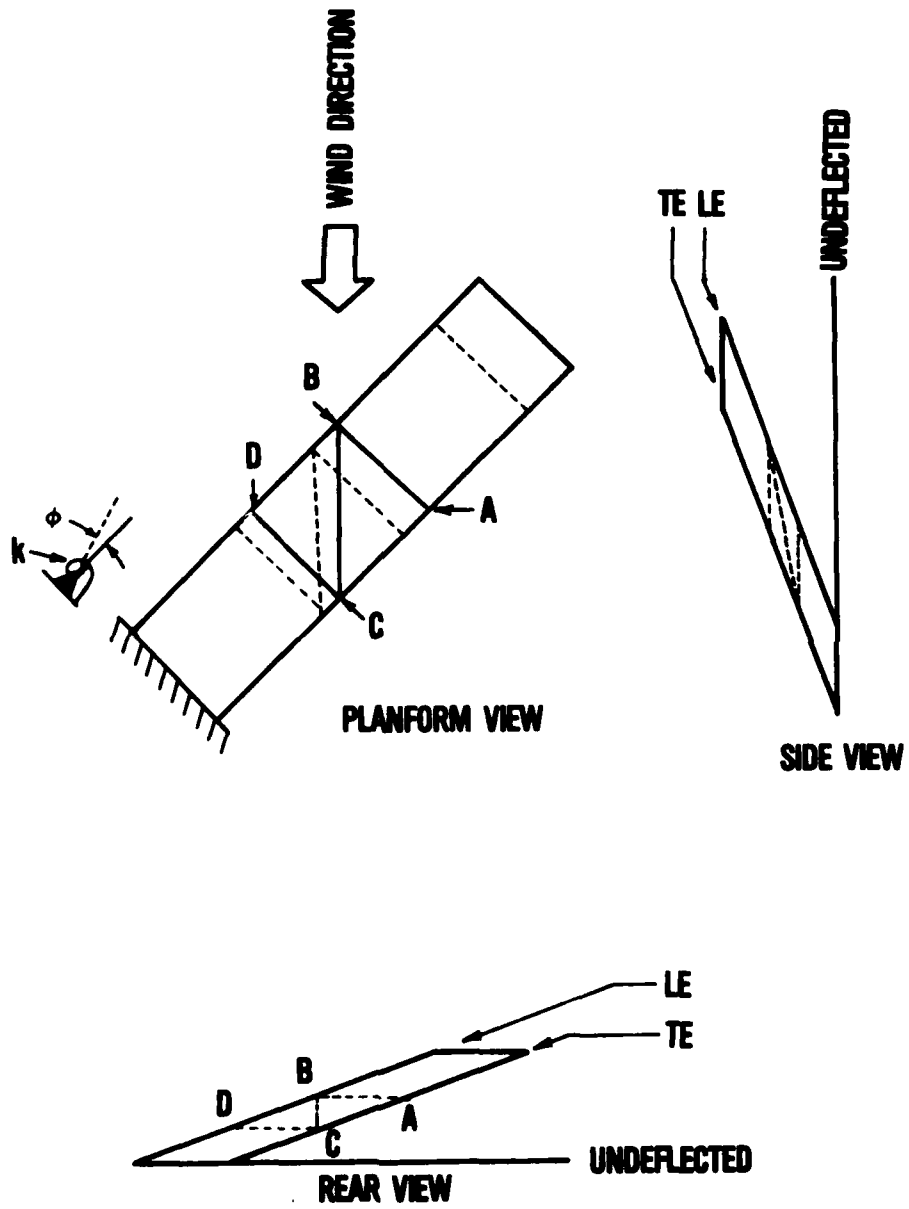
Figure 5.   A View of Deformation Related Angle-of-Attack for a Forward
            Swept Structure

The larger the load, the larger the deflection component angle-of-attack becomes. In effect, forward swept wing deformations contribute to pressure loads on the wing.

If wing tip deflection of a forward swept wing with a finite divergence speed is plotted as a function of airspeed, a relationship very much the same as Figure 3 would be obtained. The zero airspeed angle-of-attack, is now represented by the wing root angle of attack, α_r. At a non-zero angle-of-attack, α increases asymptotically to infinity as the speed approaches the divergence speed. As it is with the two-dimensional wing, one needs to orient the forward swept wing with zero angle-of-attack to physically reach divergence without a premature overload. At zero angle of attack no aerodynamic loads are generated until the divergence speed is reached at which time the wing will become statically unstable.

The relationship between α and q at constant lift may be used as a means of subcritically determining an experimental value of wing divergence speed. Using the equation of equilibrium for the two-dimensional wing section of Figure 2, the following relationship results:

$$q\alpha_0 = (\frac{-eS}{k} \; \frac{dC_L}{d\alpha} \; q\alpha)q + \alpha q. \tag{7}$$

The product of α times q may be considered constant if wing lift is held constant because the lift equals $(\frac{dC_L}{d\alpha})qS\alpha$. The above relationship is the equation for a straight line with $q \cdot \alpha_0$ on the ordinate and q on the abscissa. By plotting experimental values of zero air speed angle-of-attack and free stream dynamic pressure while maintaining constant lift, a family of points will lie on a straight line that crosses the abscissa at the divergence q. This method may be used in the subcritical region by extrapolating divergence q before reaching this critical value. This method may be extended to subcritical testing of a finite swept wing. However, data obtained in tests reported later herein show that

13

a plot of $\alpha_r \cdot q$ as a function of q is slightly curved and a second order fit of the data points must be used.

The growing need for static aeroelastic analysis was recognized by Flax in 1945 in a paper (Reference 15) wherein he suggests some areas for further research. One noteworthy observation of his establishes similarity between the two-dimensional equation for static aeroelastic stability (Equation 3) and Southwell's equation for column buckling. Taking Flax's suggestion, Southwell's approach has been used for experimental projection of divergence dynamic pressure (Reference 13). Southwell presented this method for beam buckling in 1932 (Reference 16) and the method, as it is used for divergence projection, still bears his name. Using the two-dimensional airfoil again and the equilibrium equation, the following alternate form comes with algebraic manipulation of Equation 3:

$$(\alpha - \alpha_0) = q_d [\frac{\alpha - \alpha_0}{q}] - \alpha_0 \tag{8}$$

For a wing with fixed α_0, this is an equation for a straight line. The abscissa is $(\alpha - \alpha_0)/q$ and the ordinate is $(\alpha - \alpha_0)$. The slope is the divergence q. By plotting experimental values of $(\alpha - \alpha_0)/q$ and $(\alpha - \alpha_0)$ according to Southwell's method, the divergence q may be subcritically determined from the straight line fit. This linear relationship was experimentally verified for a two-dimensional wing section in Reference 17.

The second subcritical method of determining divergence q may be extended to the testing of swept finite wings. The basis for this was presented in Reference 18. Using untapered beam theory and aerodynamic strip theory, a linear relationship may be derived which shows the relationship between wing deformation and dynamic pressure. However, closed form expressions are unknown for finite swept wings with taper and sophisticated aerodynamics. Evidence of the theoretical validity of Southwell's method for more sophisticated swept wings will be presented in the next section of this report.

SECTION III

COMPUTATIONAL METHODS AND THE DESIGN PROCESS

A method of analysis has been suggested by Weisshaar in Reference 19. With this method, a computer program with the acronyms CWING was developed to analyze a cantilevered composite wing with a segmented beam like structure. Each structural element has bending stiffness, torsion stiffness, and a bend/twist coupling factor. Using finite element formulation techniques the structural stiffness matrix was formulated by Weisshaar for the CWING program. Aerodynamic lift on each structural element is generated by a horseshoe vortex aligned with the local aerodynamic quarter chord. An aerodynamic stiffness matrix is generated in CWING which is a direct function of q. In essence, CWING generates the matrix equations of equilibrium and determines the static deformation for a given speed and root angle of attack. For divergence analysis, the equations are treated as an eigenvalue problem with q as the eigenvalue. Using standard matrix methods of eigenvalue solving, the lowest eigenvalue is calculated which is the critical divergence q.

For the purpose of this report, four programs were written which use the CWING program as a basis. These programs are qiven names of One, Two, Three, and Four. A description of these programs is qiven below.

Program One was used to numerically demonstrate the application of Southwell's subcritical method of experimental divergence projection for a swept wing. The CWING derived equations of equilibrium of a specific wing were solved for bending moment at various values of dynamic pressure. Root bending moment, M, was then plotted as a function of M/q. This is a modified function of the Southwell method shown in Equation 8 where $(\alpha - \alpha_0)$ is plotted as a function of $(\alpha - \alpha_0)/q$ for a two-dimensional wing. For a finite swept wing, Equation 8 suggests that for divergence projection with the Southwell method, one plots $(\alpha - \alpha_r)$ as a function of $(\alpha - \alpha_r)/q$. Linear elastic theory suggests that root bending moment will be proportional to the elastic angle of attack. Local

angle of attack is a difficult parameter to measure on an aeroelastic wind tunnel model. Root bending moment can be measured with the use of a strain gauge. Therefore, it is reasonable and desirable to project divergence speeds with Southwell's method using bending moment and dynamic pressure (References 10, 11, 12, and 13). Evidence of Southwell's method and its validity is provided by Program One and the result is shown in Figure 6. Here, the wing structure model has similar dimensions and stiffness as the experimental wing which was built for this project.   The slope of the line in Figure 6 is 0.284 psi. The divergence q predicted by CWING using its eigenvalue technique is 0.282 psi. The difference between the simulated Southwell method and the CWING eigenvalue solution is less than one percent. These results suggest that a theoretical basis of the Southwell method for the projection of divergence with finite swept wings is present.

Program Two was developed to numerically demonstrate the constant lift method for subcritical divergence speed determination, which was described in the review of the divergence phenomenon. Program Two uses the matrix equations of equilibrium developed for CWING and determines the root angle of attack required to maintain constant lift at varying dynamic pressures. The quantity q times α_r is plotted as a function of q. The result is shown in Figure 7 for the same wing which was used for the Southwell verification of Figure 6. As noted earlier, the line is not straight and requires a second order fit. However, the divergence q projected by this constant lift simulation is 0.282 psi, exactly the calculated value using the CWING program eigenvalue technique. This is expected since the divergence condition for this wing will only be reached when the root angle of attack is zero.

Program Three and Program Four were written to generate design curves for the wing to be constructed for wind tunnel testing. These programs used a slightly modified CWING program enclosed in Fortran Do Loops to calculate divergence speeds for a full range of sweep angles and wing skin fiber orientations. With the assistance of a computer graphics display, results were quickly and easily analyzed. Due to the short computer turn-around time inherent with CWING and the graphics
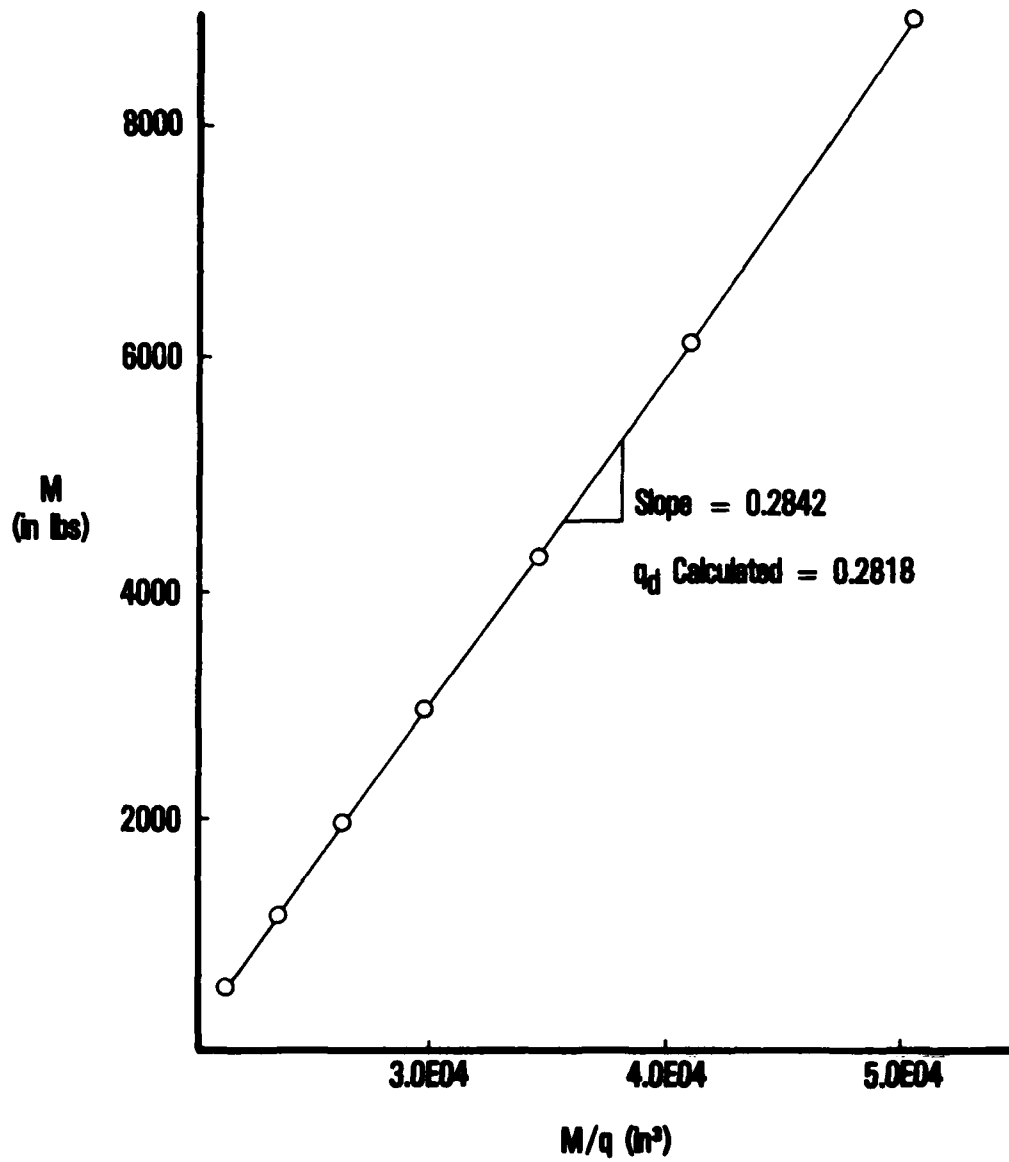
Figure 6.   Southwell Plot Simulation
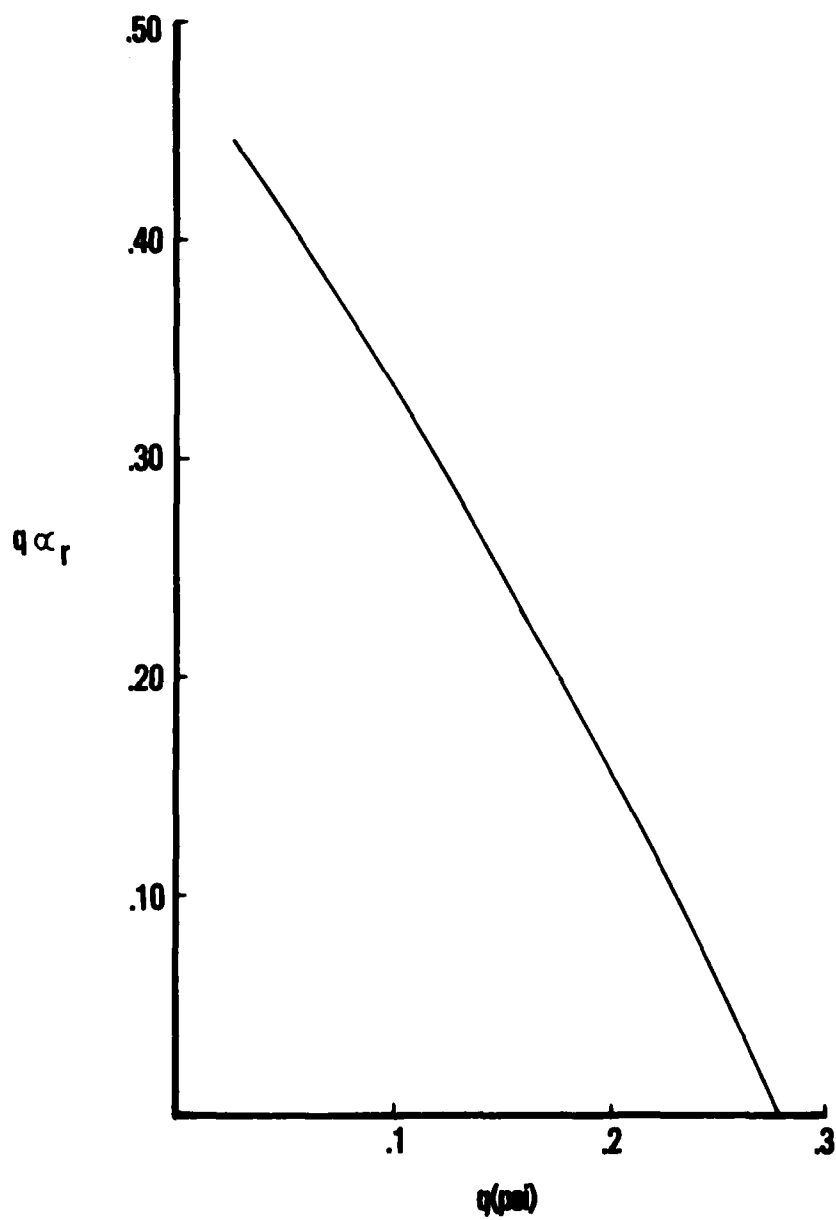
Figure 7. Constant Lift Method Simulation

display, a feasible wing design could be established for aeroelastic wind tunnel testing. This method of aeroelastic tailoring provided an excellent educational experience because optimizing decisions were provided by the designer.

A design was chosen which would be suitable for divergence testing over a range of sweep angles and fiber orientations. Many constraints were considered. The foremost constraint required the divergence speeds to fall within certain wind tunnel velocity bounds. Other constraints employed were aerodynamic and plate planform size and plate thickness.

A preliminary wing span of 40 inches was chosen in order to fit within the Virginia Tech 6 foot wind tunnel without aerodynamic inter- ference effects. The chord and aspect ratio were chosen arbitrarily. Plate thickness was very important in determining the wing stiffness, thus ensuring wing divergence speeds which were within the wind tunnel velocity range. For the purpose of sizing the wing, it was assumed that the plate was cut from a 1/8 inch aluminum sheet. Simple equations in Reference 6 provided a means by which an estimated divergence speed could be determined. With the use of the aforementioned computer programs, the design was refined. The design process became more exacting when composite material was substituted for aluminum. Decisions which concerned ply orientation and stacking sequence were not easily resolved. The final design utilized a core layup with no bend/twist coupling. Off axis plies were added to the outer surface of this core to introduce bend/twist coupling. When reference is made to plate fiber orientation, only these off-axis ply orientations are referred to. With the preliminary design description now completed, details of the model construction are given in Section IV.

Parameter curves which relate divergence q to wing sweep and fiber orientation are presented in Figure 8. These curves are descriptive of the preliminary wing design only. Sweep is plotted on the vertical axis and fiber orientation is shown on the horizontal axis. This plot may be viewed as a three-dimensional surface where the dimension normal to the page represents divergence q. Each curve on the page represents a constant limit q for the design of a divergence critical wing.

19
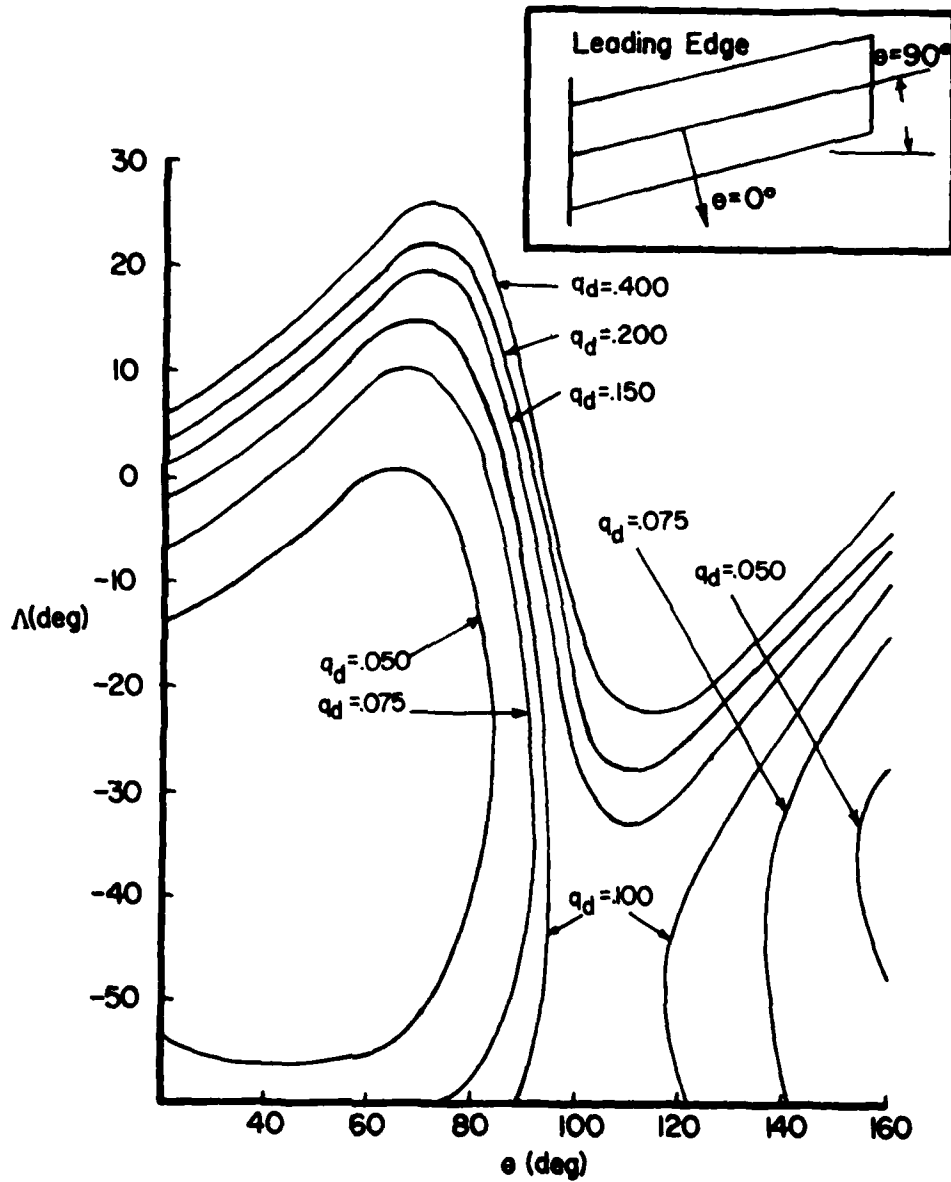
Figure 8. Design Curves; q_d Plotted as a Function of Sweep and Fiber Orientation

The relationship between sweep and q_d for constant fiber orientation is presented by a slice perpendicular to the fiber orientation axis. These relationships are shown in Figures 9, 10, and 11. Each line in these figures represents a plate with constant fiber orientation, θ, which was to be wind tunnel tested. In all cases the anticipated divergence q was minimum between 50° and 25° forward sweep. Each case becomes divergence free as the wing is swept aft from this minimum point.

A slice from left to right of Figure 8 gives the relationship between fiber orientation and divergence q for constant sweep. Maximum stability is reached between orientations of 100° and 120°. This trend was also expected to be found in the experimental results.

These curves represent only a preliminary analysis. As will be explained, several parameters which were introduced in the experiment could not be modelled by procedure CWING.
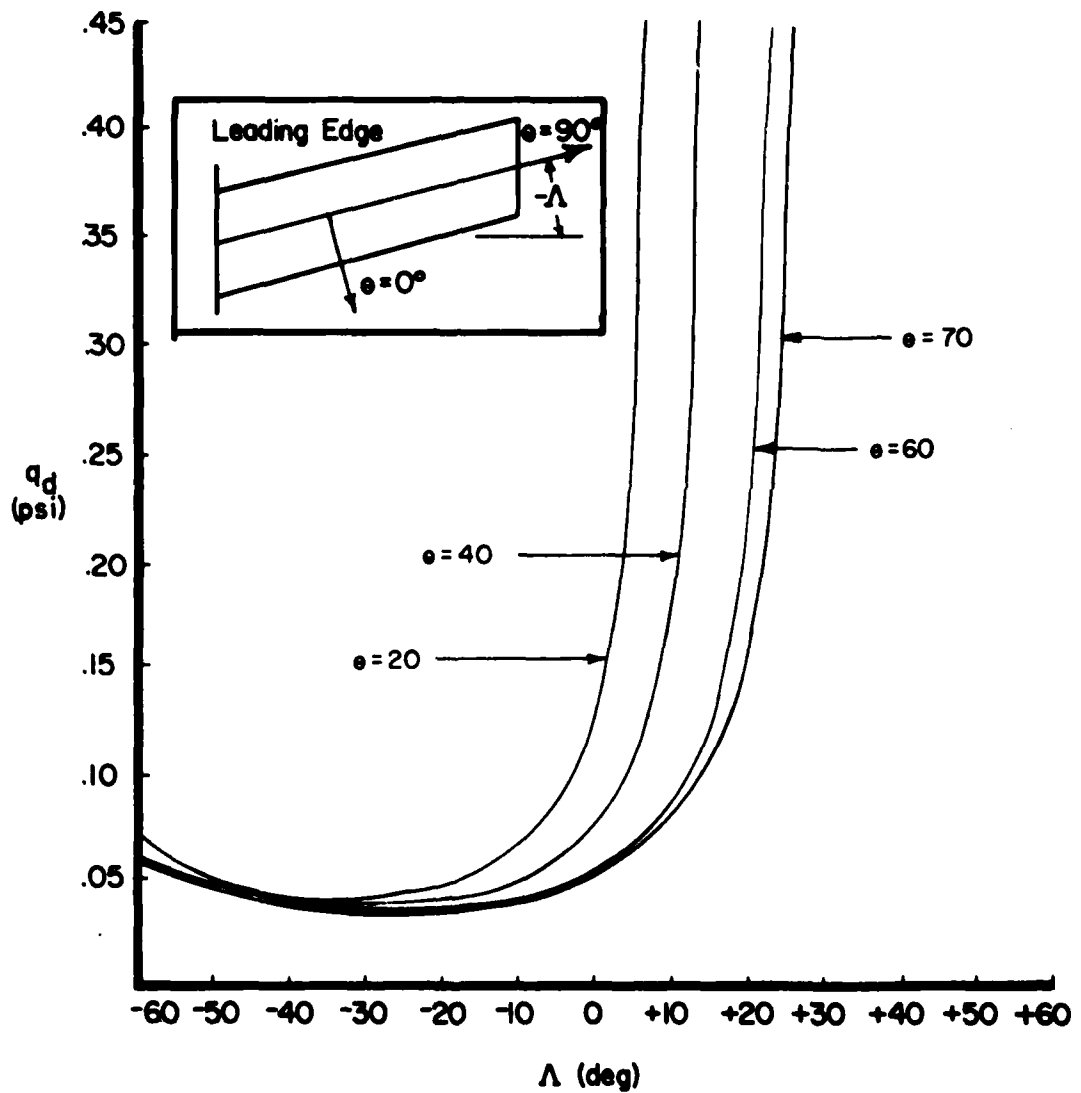
Figure 9. Design Curves; q_d as a Function of Sweep for Fiber Orientations of 20°, 40°, 60°, and 70°
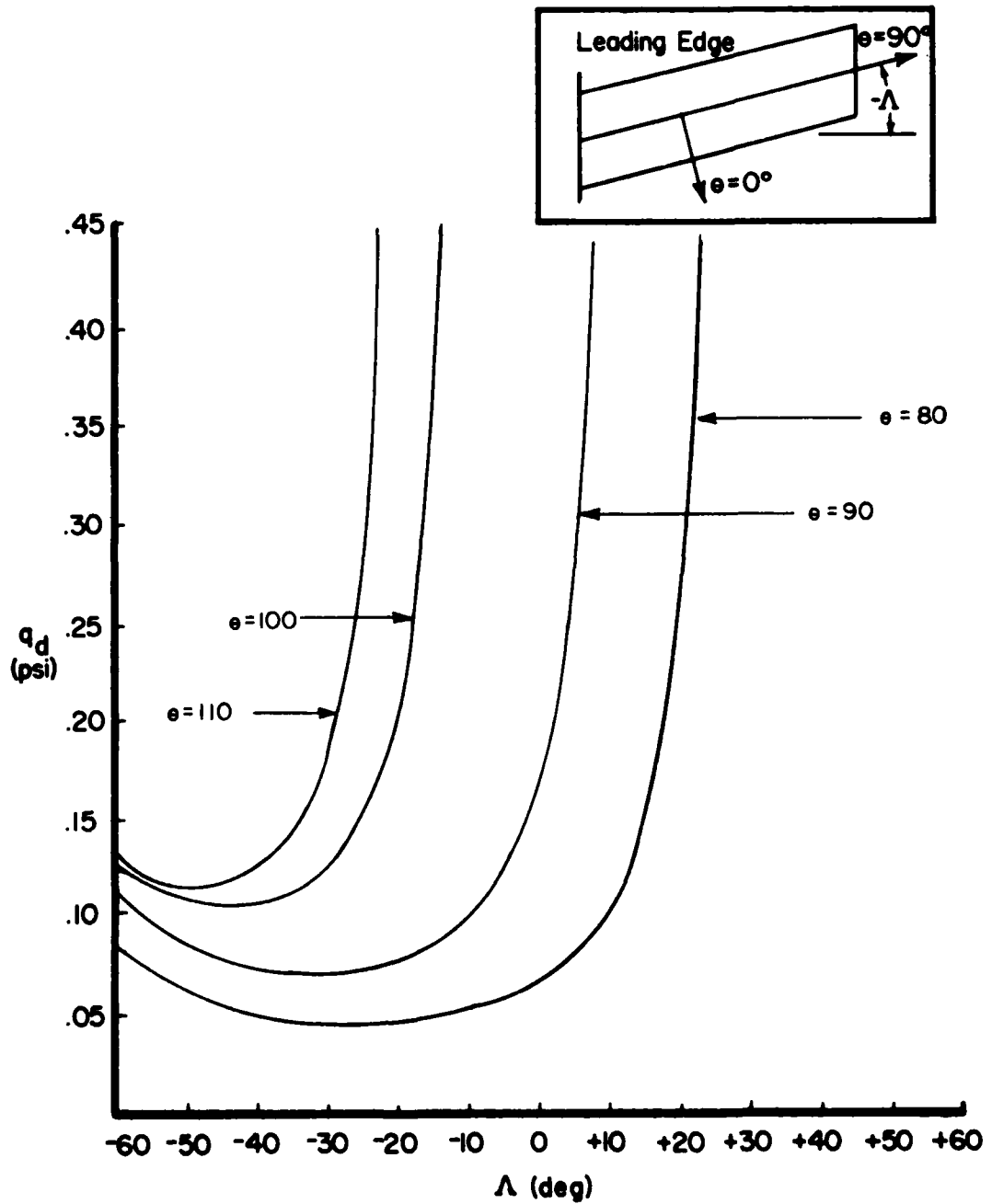
Figure 10. Design Curves; q_d as a Function of Sweep for Fiber Orientations of 80º, 90º, 100º, and 110º
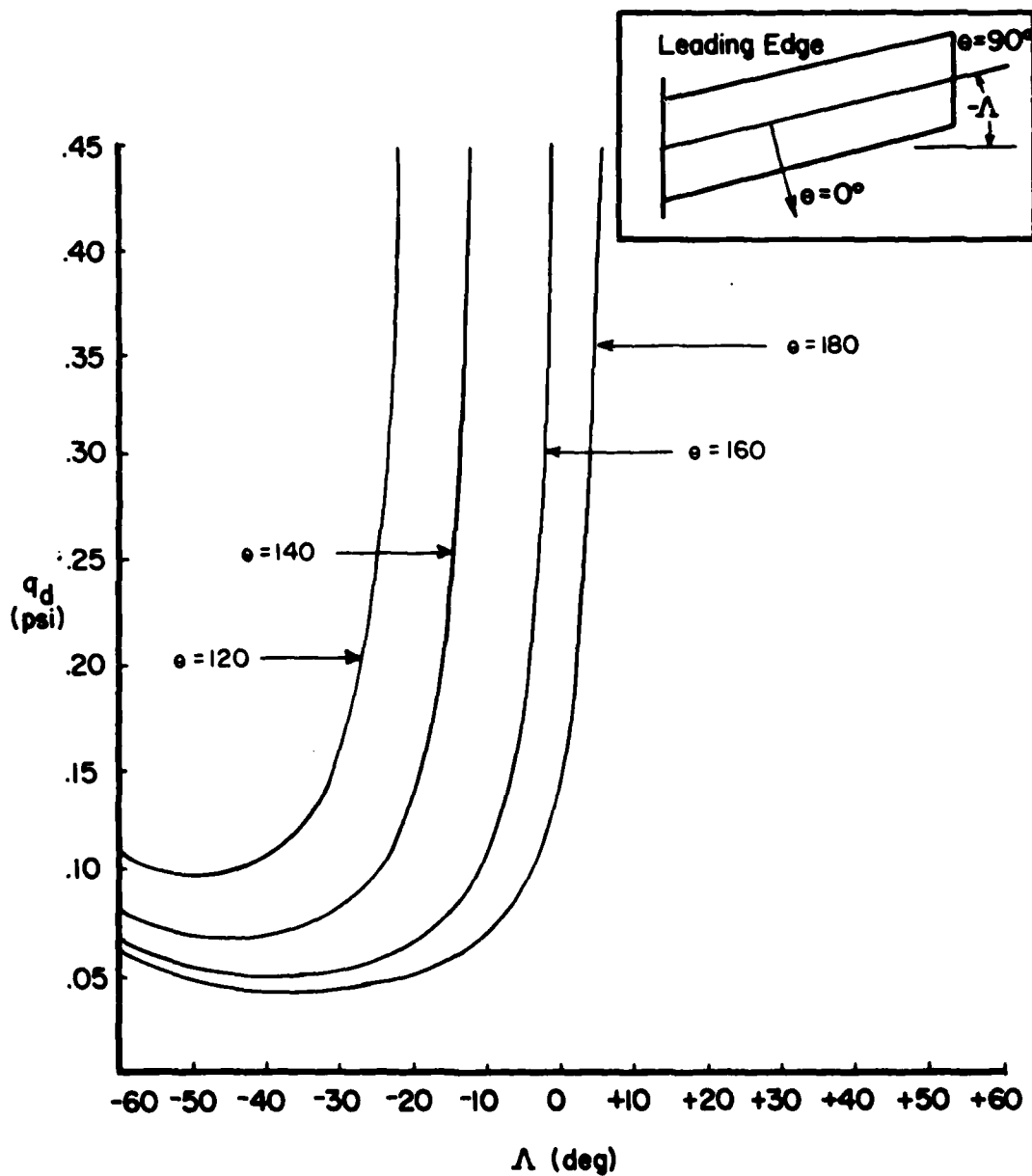
Figure 11. Design Curves; q_d as a Function of Sweep for Fiber Orientations of 120°, 140°, 160°, and 180°

24

SECTION IV

MODEL CONSTRUCTION

The purpose of this project was to show relationships between wing sweep,fiber angle, and divergence speed. To gather the most data for the least cost, it was necessary to devise a model that was inexpensive and also required only a short delay to change configurations. In addition, aeroelastic instability was to be enhanced so the wing divergence speeds would fall below the maximum useful wind tunnel speed.

A high aspect ratio plate may be designed with sufficient flexibility to allow wing divergence at low speeds. However, a plate with sufficient thickness to aerodynamically represent a similar full scale wing is far too stiff. Stiffness increases rapidly with thickness. While a full scale forward swept wing may likely diverge, it was felt that the aerodynamic shape and structural stiffness should be modeled independently to demonstrate this phenomenon on a smaller scale and at low speeds.

A model was designed with a sectioned aerodynamic shell. It was attached to and enclosed a removable plate with high aspect ratio. This concept, shown in Figure 12, was previously used with success by the Flight Dynamics Laboratory (Reference 12). Because the plate was removable, various plates could be designed for use in the shell, thus allowing variable fiber angle.

The plates were made with graphite epoxy AS5301 prepreg tape. Each plate contained the same central core layup. Unique to each plate were the two outer ply orientations. It is these two outer plies that determine the anisotropic quality of the plate. These plates were free to flex inside the aerodynamic shell. Each shell section was connected to the plate with an internal bridge. The bridge held the shell to the plate when two screws were tightened. In this way distributed aerodynamic load was transferred from the aerodynamic shell to the plate through a small contact area. This area was designed small to minimize

25

Figure 12. Aeroelastic Model in Test Stand

the restriction of plate flexibility, yet large enough to keep the shell securely in position.

The plate layups are shown in Figure 13. The central core of each plate contained the same plus and minus 45° and 90° fiber layups. Cover plies with only one fiber orientation were applied to the top and bottom of the core of each plate. It is these four other off-axis plies which gave the plates their anisotropic behavior. Orientations of 20°, 40°, 60°, 70°, 80°, and 90° were to be constructed. Because of plate symmetry, the plate could be inverted and orientations of 100°, 110°, 120°, 140°, and 160° could be tested.

Two steps were taken to cure the plates. Initially, 20 layers of five mil graphite epoxy were laid out as a large sheet to make a common core for all six plates. The core material was then cured in a vacuum bag and autoclaved. The sheet was cut to six nominally oversized plates and adhesive was applied to each side. Two outer plies of five mil graphite epoxy were then laid on each side and the composite was again cured. Due to the two step procedure and the problem in tolerance, the thickness of the core was between 0.105 in. and 0.110 in. and the thickness of the finished plates was a nominal .144 in. During the final curing process, fibers of the outer plies shifted slightly such that in the region near the leading and trailing edges the fibers rotated between zero and ten degrees toward the chordwise direction. This problem was least for the plates with plies of 90° and 20°. Due to a tight test schedule, it was decided that these plates could still be used with the understanding that they might not be truly representative of a specific flight article. It was felt that the basic relationship between sweep, fiber orientation, and q_d could still be adequately demonstrated.

The fiberglass shell was constructed over a styrofoam core which was formed using a hot wire cutter. Styrofoam core techniques are described in detail in Reference 20. Two layers of fiberglass were used to make a skin around the styrofoam core. Figure 14 shows the process by which the fiberglass shell was constructed. The first layer of
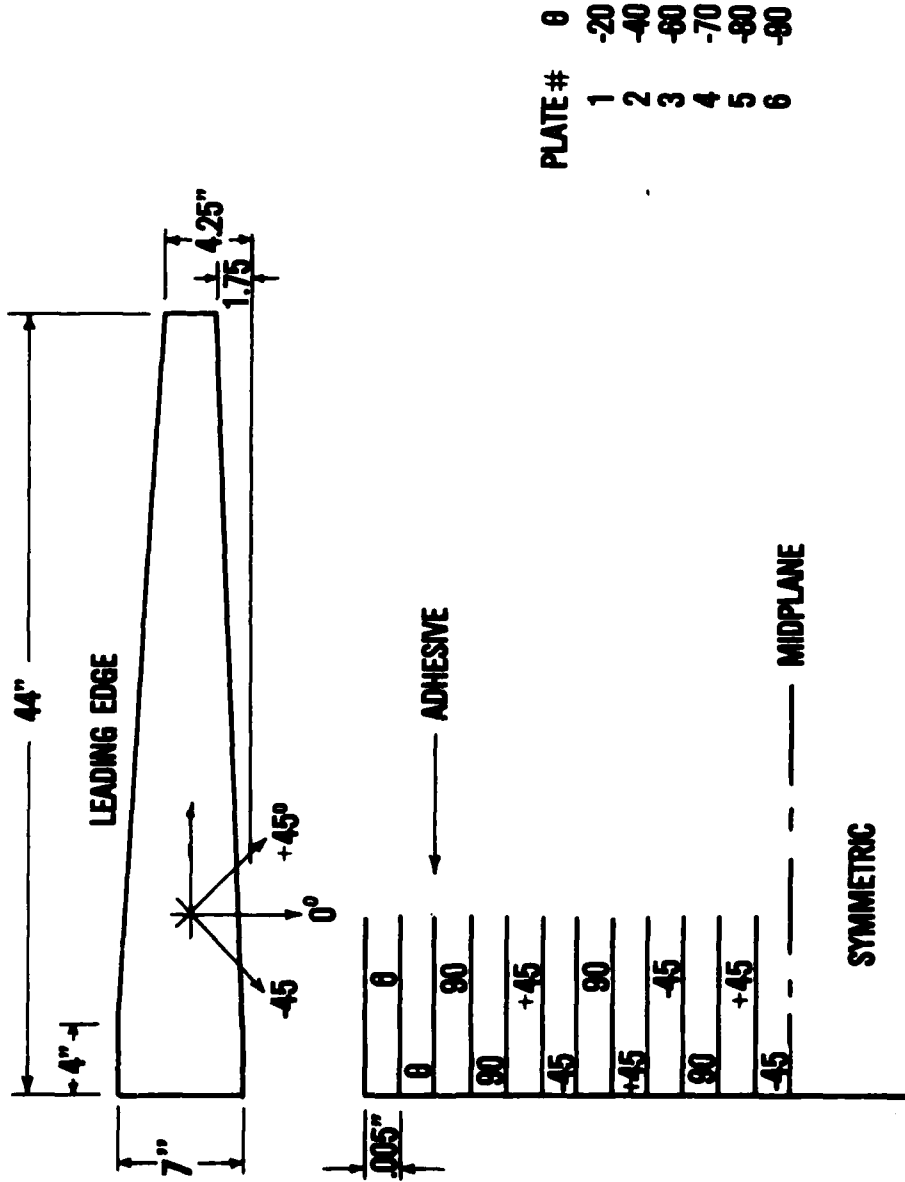
Figure 13. Composite Laminate Layups
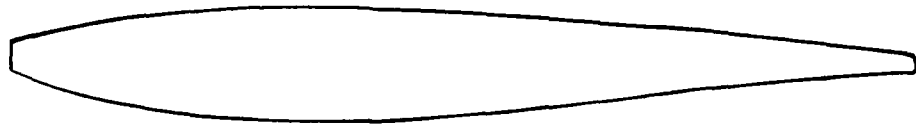
Step 1: Styrofoam Core

Step 2: First Layer Of Fiberglass

Step 3: Leading And Trailing Edges
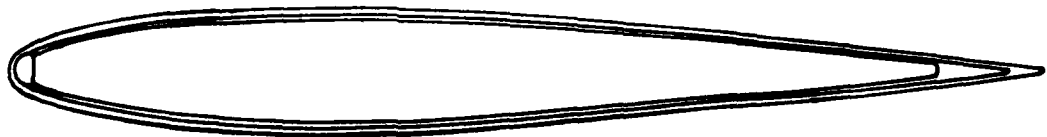
Step 4: Second Layer Of Fiberglass

Figure 14. Fiberglass Shell Construction Sequence

fiberglass was hardened using a white water-based glue. Leading and trailing edges of balsa were then glued on and sanded to shape. A second layer of fiberglass was hardened with an epoxy glue. The trailing edge was trimmed and the surface was smoothed with auto body putty and sanding. The wing tip was molded with balsa and body putty.

The wing design is shown in more detail in Figure 15. The wing was 43.5 in. in length with a 14 in. root chord and a 7 in. chord at 40 in. outboard. A constant NACA 0012 airfoil section was chosen. The span-wise line of 30% chord points is perpendicular to the root chord line but is not the reference axis.

The wing was then sectioned by removing 1/4 in. chordwise strips every 4 in. of span. The wing tip section was longer as shown in Figure 15. The 10 sections were then hollowed such that no styrofoam remained within. The 1/4 in. strips which were removed were replaced by soft foam rubber which was cut flush to the wing surface with the hot wire cutter.

Brass bridges, as pictured in Figure 16, were constructed. Due to the tapered thickness of the aerodynamic shell, two types of bridges were used. The two inboard sections contained bridges which contacted only the center of the plate. This was done by inserting 1.5 in. spacers between the bridge and the plate. Other than this detail these two inboard sections were the same as the others.

The remaining eight sections contacted only the leading and trailing edge of the plate because the bridge bowed out at the center when clamped. For expediency, the ten bridges were connected to their respective aerodynamic shell sections with body putty. Holes were drilled in the fiberglass shell to allow access to the Allen head screws which tightened the bridges.

The shell sections were slipped onto the plate and secured. A jig was used to ensure that the sections were oriented in the same position each time. This jig had three pegs which aligned the plate and a rim
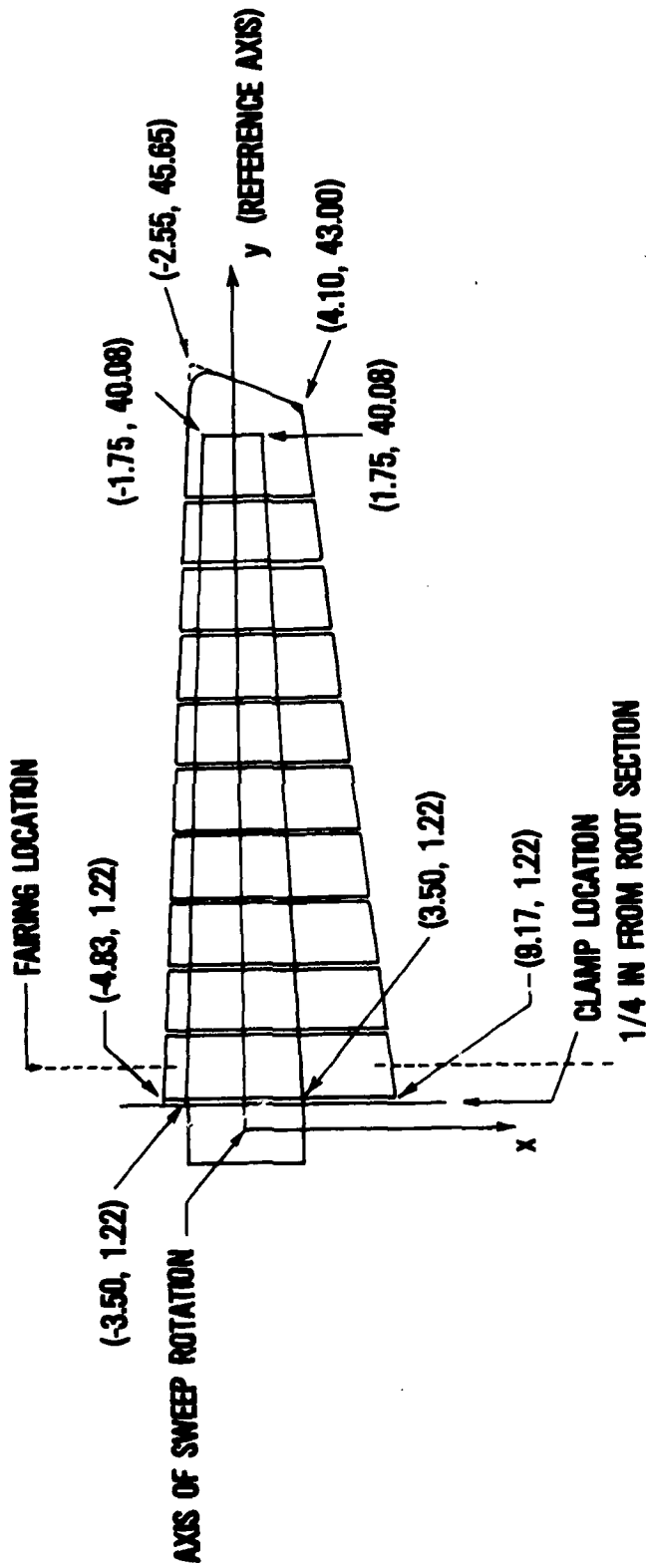
Figure 15. Planform Schematic of the Model

SPACERS INSERTED HERE
FOR 2 INBOARD SECTIONS

PLATE

BRIDGE

FRONT SCREW

FRONT PRESSURE POINT

REAR
PRESSURE POINT

REAR SCREW

■ HARDENED PUTTY
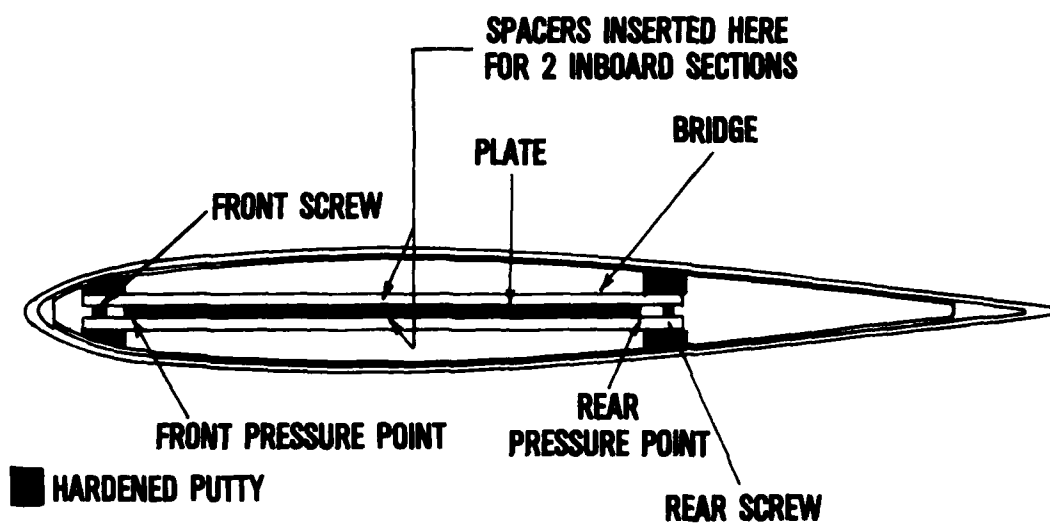
Figure 16. Typical Section of the Model

32

against which the trailing edges of the sections rested. This rim was marked to ensure the sections were located in the correct spanwise location. Figure 17 shows the wing being aligned in the jig and the shell sections secured.

A mount was designed and constructed out of steel to give the wing a cantilever support. This is shown with the wing installed in Figure 12. This mount clamped the root of the plate and allowed the wing to be adjusted and secured at various sweep angles. The mount rested on a turntable located under the wind tunnel test section. Figure 18 shows the wing in position in the wind tunnel and superimposes the -15°, -30°, -45°, and -60° configurations.

A fairing was constructed to give smooth aerodynamic flow around the mount and root of the wing. The design of the fairing was not initially given extensive consideration and caused some difficulty in determining its contribution to the experiment. The fairing's position with respect to the wing in the wind tunnel is shown in Figure 18.

One strain gauge was applied to each plate near the root to measure bending strain. This bending strain could be used to maintain a constant moment for the constant lift analysis or used for a Southwell plot.

Figure 17. Model Assembly in the Jig
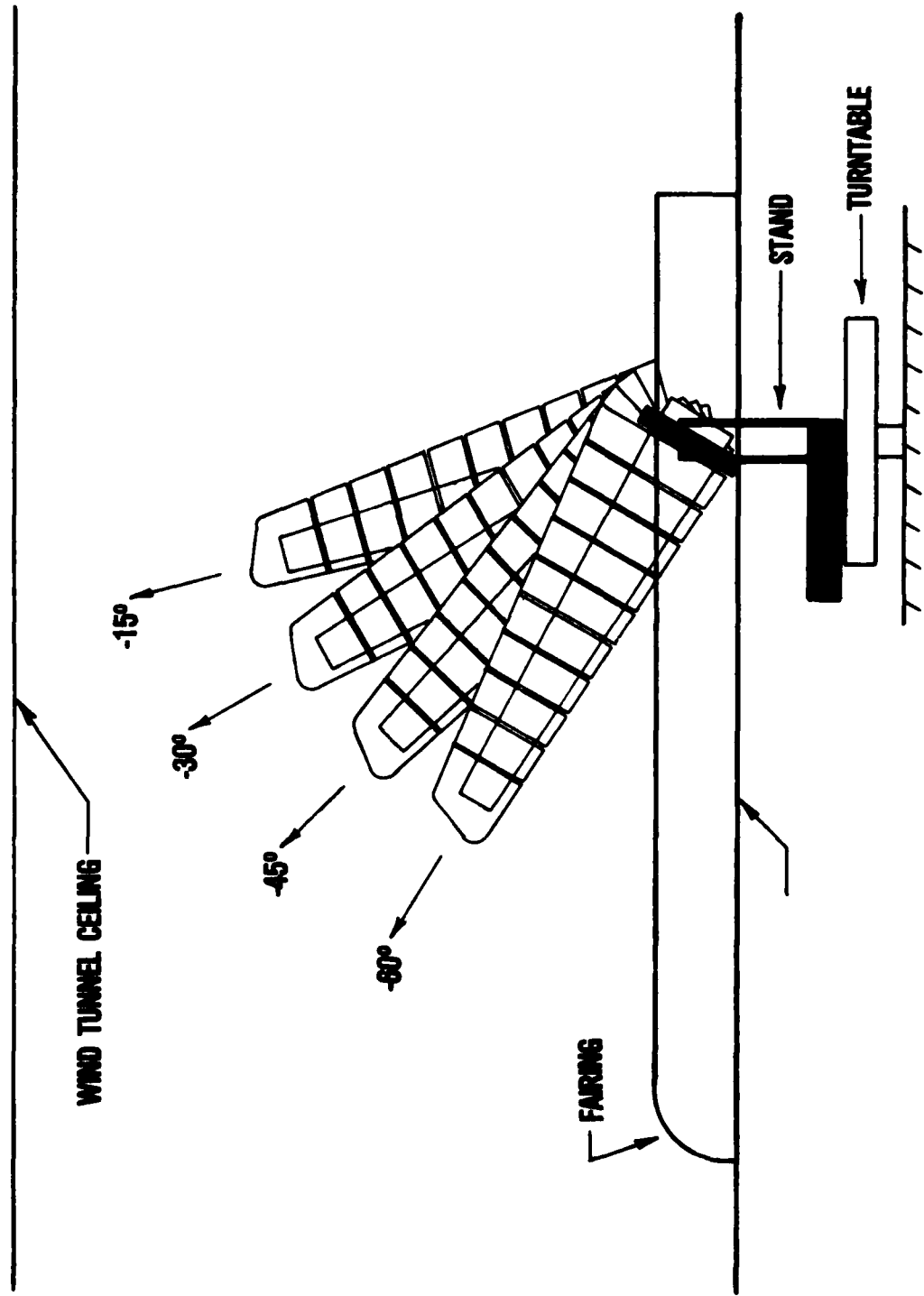
Figure 18. Configurations for Wind Tunnel Testing

SECTION V

EXPERIMENTAL SETUP AND PROCEDURE

Testing was performed in the Virginia Tech 6 by 6 foot stability wind tunnel. The wing was floor mounted as shown in Figure 18 to reduce gravity effects on wing deflection. The turntable on which it was mounted was remotely adjusted to within 1/100 of a degree angle-of-attack.

A Wheatstone bridge was constructed using 350 OHM dummy strain gauges as resistors. The change in voltage output across the bridge varied linearly with strain. A Hewlett Packard 3052A Data Acquisition system was used to sample this output. An HP 9225A Calculator automatically read in these sampled values and stored the average. Tunnel dynamic pressure, temperature and static pressure were also measured and read into the data acquisition system. The calculator used these values to calculate experimental divergence q and divergence speeds by Southwell's method discussed previously in Section II and the constant lift method. The method of least squares was used to fit a second order curve for the constant lift data and to fit a straight line for Southwell's method. An HP 9872A digital x-y plotter was used in conjunction with the calculator. This machine plotted data points as they were taken, thus enabling on the spot decisions to be made. When all data was input, a line was automatically fit through the set of points and the final calculated value of divergence q was printed out. A schematic of this operation is shown in Figure 19.

A video camera and monitor were run constantly to record any unusual phenomenon. A 16MM movie camera was used to film the response of the wing at the divergence velocity.

Except for the adjustment of the wind tunnel speed, Southwell's method was totally automatic. The first plots with the constant lift method required many data points which took much time. In addition, angle-of-attack setting for constant lift became difficult near the
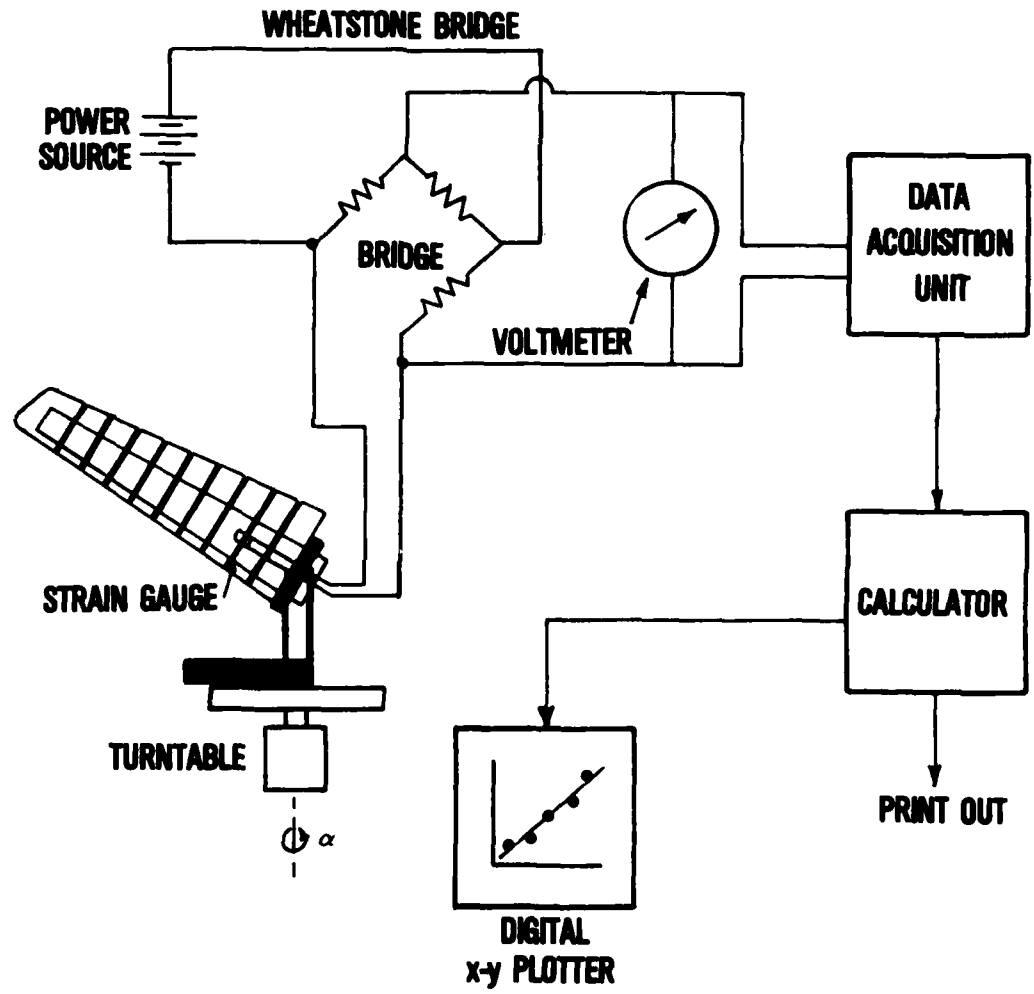
Figure 19. Data Acquisition Schematic

divergence speed due to the wing's aeroelastic sensitivity. Thus, because exclusive use of Southwell's method would save time and due to the excellent straight line fits which results, only the Southwell method was used throughout the remainder of the test.

A procedure for adjusting the wing and taking the data was established after several runs. The pivot point on the stand was tightened and the wing was clamped with a 1/4-inch gap between the inboard shell section and the clamp. Once clamped, the pivot was again loosened and adjusted to the desired sweep angle and tightened again. The angle of sweep was measured with an inclinometer which was aligned with the leading edge. When the inclinometer measured three degrees aft sweep, the wing reference was at zero degrees. This three-degree angle between the leading edge and the reference axis is apparent in Figure 15. It was discovered that plate thickness was not entirely uniform in the chordwise direction and allowed some flex within the clamp. This problem was acknowledged but not analyzed.

With the wing secure, strain gauge wires were reconnected and the voltage output was given a quick check. The fairing cover was installed so that a nominal 1 to 2 inch gap remained between the slot's edge and the wing surface. The wing was then ready for a divergence test.

Using analytical predictions, an initial wind tunnel speed was chosen. Data was taken by the calculator and values were plotted according to Southwell's method. After the second data point was taken, updated values of projected divergence q were printed by the calculator to avoid unanticipated wing divergence. Wind tunnel testing could be performed at near divergence speeds, thereby ensuring more accurate projections. This feature of the test system was incorporated after a near disaster which will be explained later.

When all wing configurations were tested, check cases were performed in the wind tunnel to verify previous experimental results. One check involved testing a wing, disassembling it, and retesting it for wing divergence. Another check involved the effect of the gap

between the fairing and wing surface. Further tests were performed to gain intermediate data points by varying sweep on the 90° plate. With the remaining wind tunnel time, plates were tested for divergence with no aerodynamic shell.

The final test was the filming of an actual divergence, and correlation of the observed divergence q with the value projected by Southwell's method. Experimental projection was made with Southwell's method just prior to the run to divergence speed. In order to diverge the wing without premature overload, a zero lift angle-of-attack was established at low speeds by adjusting the turntable. As the speed was increased, it became impossible to maintain zero lift. The forward swept wing would bend one way or the other depending on perturbations. As the wing approaches its divergence velocity, its restoring potential decreases, as was explained in the review of the divergence phenomenon. That is, while the structural stiffness remains constant, the aerodynamic stiffness increases linearly with dynamic pressure and reduces the apparent stiffness. This phenomenon becomes understood as one witnesses the apparent lack of overall stiffness near the divergence speed. In other words, the wing looses its ability to resist small changes in the flow and seems to float about its equilibrium point. Thus, the zero root angle-of-attack could not be guaranteed at higher speeds. Therefore, the speed at which the wing overloaded was likely close to, but guaranteed to be lower than the divergence speed. (One may note that in Reference 16, Southwell identified a similar problem with respect to the destructive testing for beam buckling.)

Due to the test schedule and limited time, static load tests were performed on the 90° plate after the wind tunnel tests. As shown in Figure 20, the wing was loaded while it was in the variable sweep mount used in the wind tunnel tests. This figure shows the wing loaded in pure torsion through a lightweight bar which attached to the wingtip chordline. Two weights and two pulleys provided the torsion as shown. Bending tests were performed with the same bar and one weight which pulled on the reference axis at the wingtip.

Figure 20. Static Test Apparatus

Using a standard 35MM projector, a grid image was shown on the surface of the wing with the wing clamped in the stand as pictured in Figure 21. Mirrors on the reference axis reflected the projected light back on a large grid board. Mirrors were locally aligned such that the cross lines of the grid image were reflected on the grid board. As the wing was loaded in bending and later torsion, structural deflection angles could be measured by the displacement of the reflected light. The cross line image on the grid board made more accurate measurements of displacement possible. The relationship between load and rate of angular deflection is given by the well known relationships for beam structures.

$$M = EI \frac{d\sigma}{dx} \qquad\qquad T = GJ \frac{d\phi}{dx}$$

By measuring local moments and local slopes due to bending, bending stiffness could be approximated. For the approximation of torsional stiffness, relations between local torque and twist due to that torque were measured.

This method assumes that twisting and bending the wing varies linearly between mirror stations. In addition, this method cannot account for structural flexibility under the mirror mounts. Soft clay was used for the mirror mount in this experiment. In spite of these limitations, this method proved reasonable.
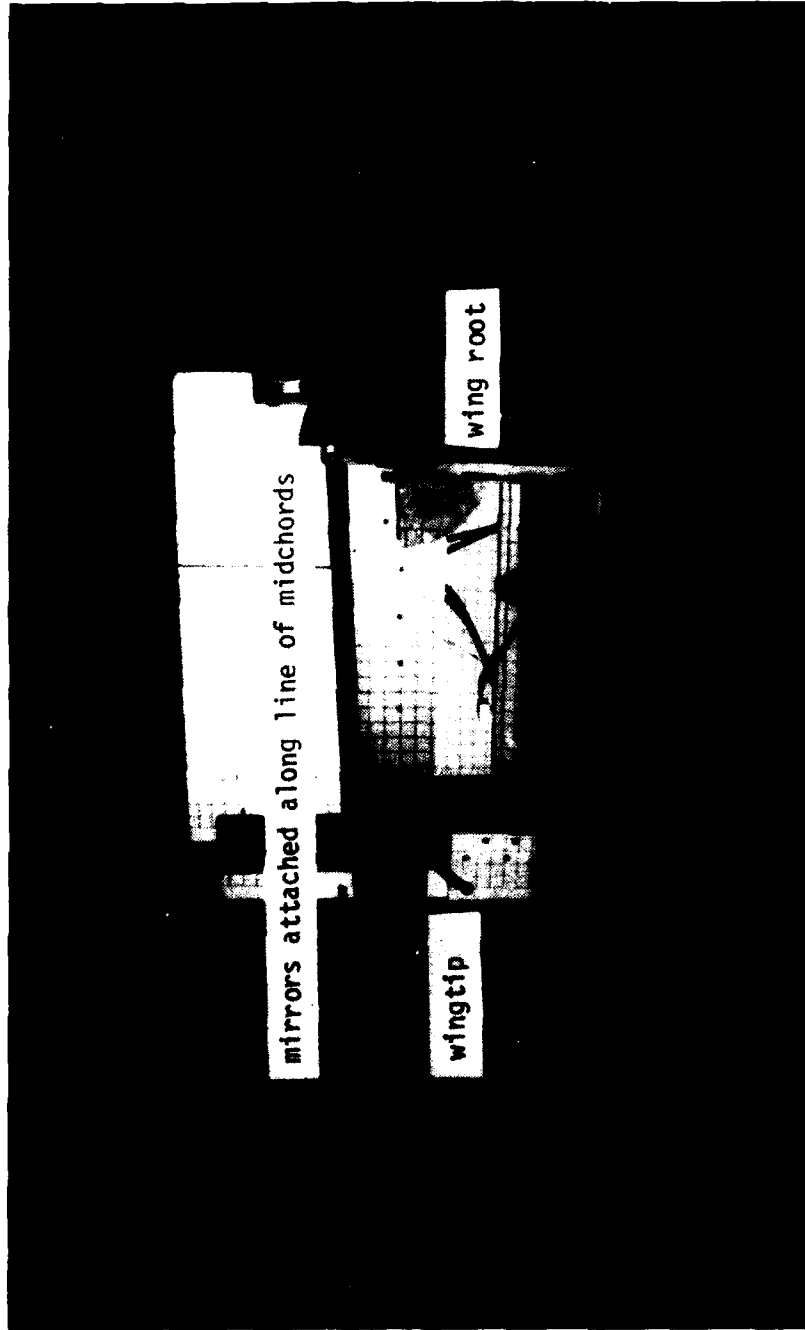
Figure 21. Grid Image on Wing Under Static Load

SECTION VI

RESULTS AND DISCUSSION

The results of the static analysis are given in the following table. Bending and torsional stiffness (EI and GJ) are directly proportional to the chord for a uniform plate with constant thickness. Thus, for this tapered plate, EI divided by chord is a constant denoted as EI/c. The same relationship is represented by GJ/c.

	EI/c (lb in)	GJ/c (lb in)
CWING (24 Plies at 5 Mil)	2541	1002
Static Test, No Shell	2779	1263
Static Test, Shell Attached	2769	1659

The bending stiffness of the plate alone is slightly higher than the plate which was designed by CWING. This was anticipated due to the differences between the design and actual thickness. With the addition of the sleeve, torsional stiffness increased to a substantially higher value than designed by CWING. This means that the sleeve was much more effective in restraining twist than bending.

During the static tests, some internal friction was noted. This was most likely attributable to the contact point between each bridge and the plate. It is assumed that while in the wind tunnel the wing was shaken sufficiently by the air flow to loosen any internal friction.

Ninety-four divergence tests were run using Southwell's method. These tests are identified by the sequence in which they were wind tunnel tested. Thus, Case 1 refers to the first test and Case 94 refers to the last test. With remarkably few exceptions, the Southwell data were linear and without scatter. This is attributed to the data acquisition system which can analyze a large amount of data in short

periods of time, thus allowing for an accurate averaging process of the test data plotted using Southwell's method. The results of the tests are given in the Appendix. Only the data points used for aeroelastic trend correlation are given in this appendix. Other runs were made to determine intermediate points and to analyze the influence of outside factors.

At this point, the reader is reminded of the reference axis used in describing fiber orientation and wing sweep. Negative sweep is associated with forward sweep. Fiber orientation is referenced to the structural spanwise axis which is denoted in Figure 15 as the reference axis. Fibers parallel to this spanwise axis are oriented in the 90° direction. Fibers which are perpendicular to this axis are oriented in the 0° direction.

A typical Southwell plot is presented in Figure 22. This represents the 30° forward swept configuration containing the 120° plate. The slope of the straight line fit is .0927 psi which is the predicted divergence dynamic pressure. In general, forward swept wings are divergence proned and as such, the Southwell plot yields a positive slope. Figure 23 presents results which for the first time show a Southwell plot with negative slope, indicating a divergence free condition. Yet this is the 15° forward swept configuration with the 120° plate. It is demonstrated here that divergence constraints can be entirely alleviated by proper orientation of the fibers for some configurations. It was interesting to note the high damping and small amount of washin associated with this forward swept configuration. These are characteristics common to aft swept configurations.

Figure 24 presents a Southwell plot for the 15° forward swept configuration with the 70° plate. Washin characteristics associated with the 70° plate were enhanced when compared to the 120° plate. For this reason, the divergence dynamic pressure is only .0477 psi. In fact, the washin characteristics were so strong that the 15° aft swept
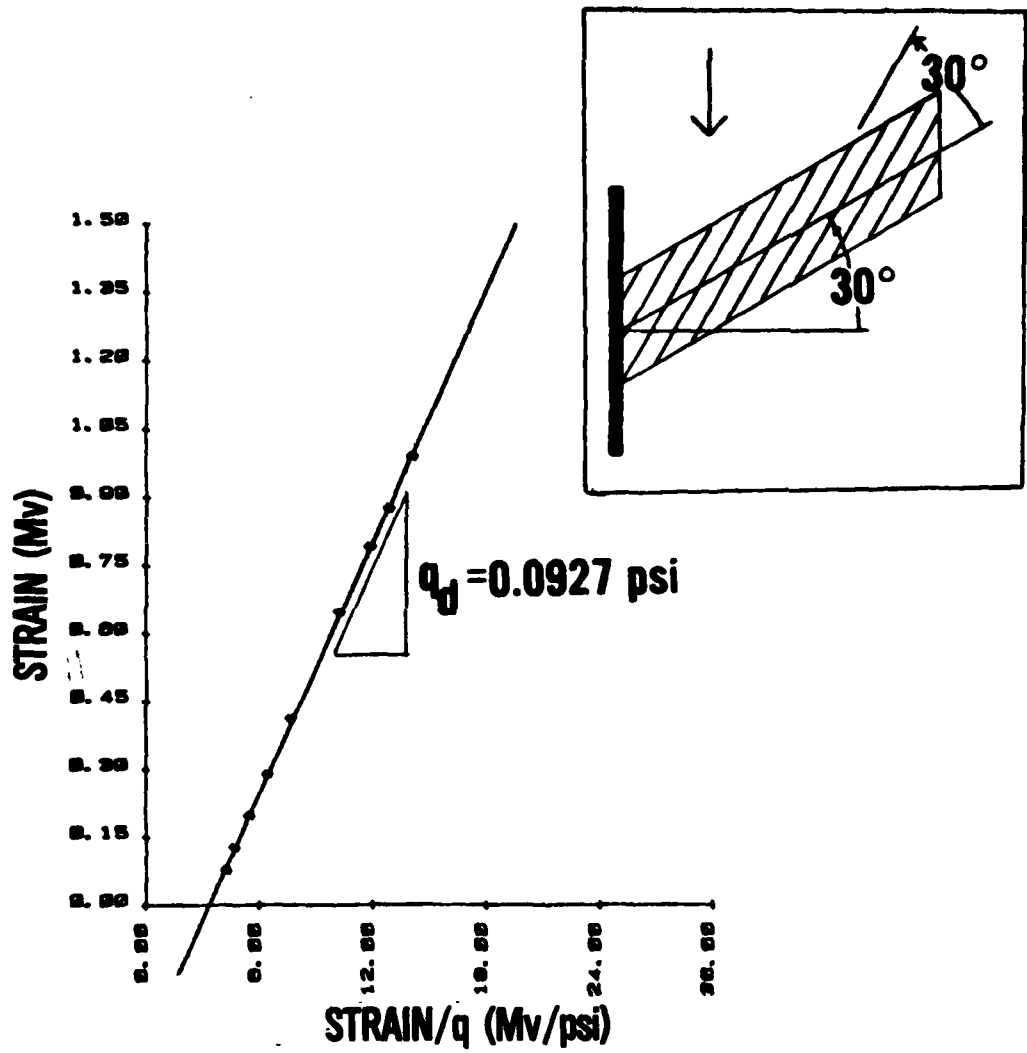
Figure 22.   Southwell Plot for the 30⁰ Forward Swept Configuration with a 120⁰ Plate
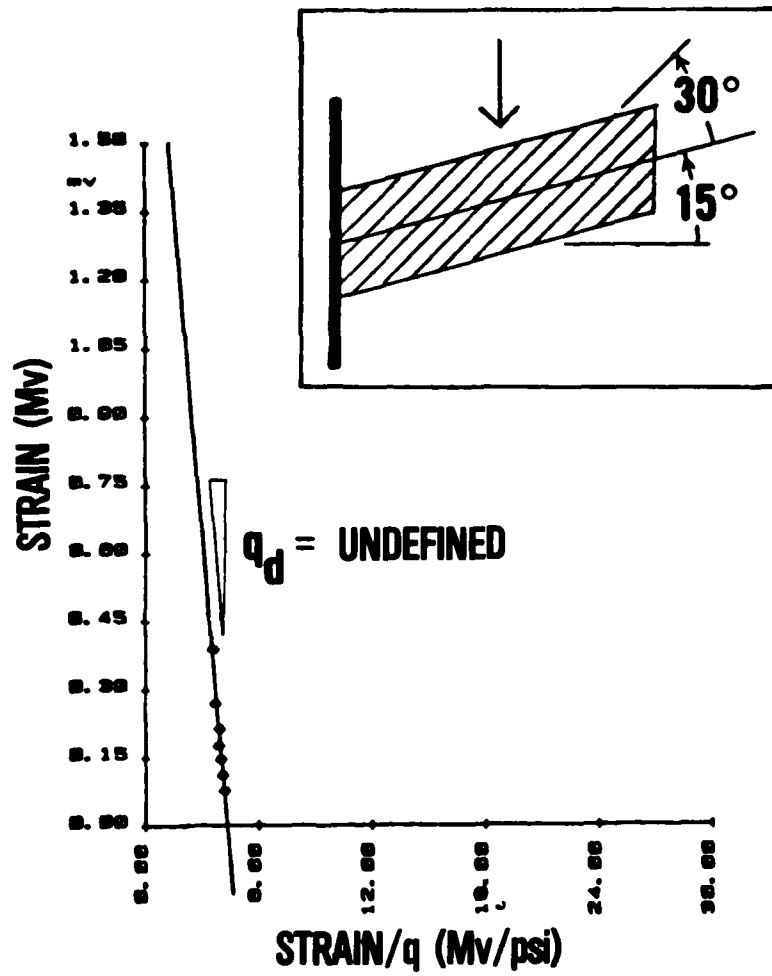
Figure 23. Southwell Plot for the 15° Forward Swept Configuration with a 120° Plate
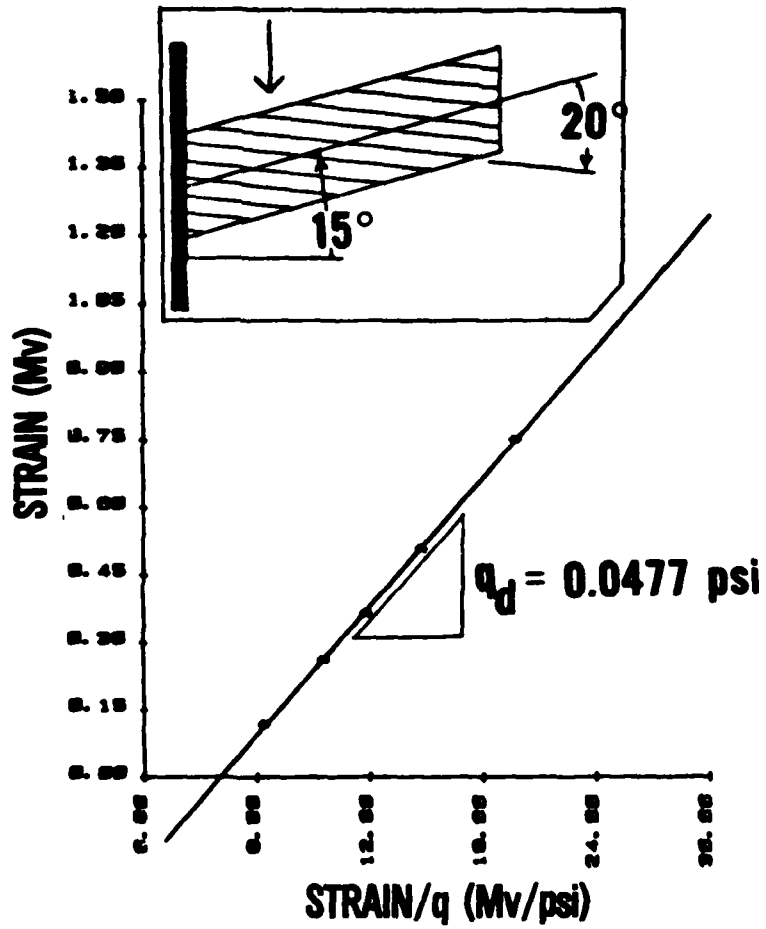
Figure 24   Southwell Plot for the 15⁰ Forward Swept Configuration with a 70⁰ Plate

configuration was predicted to have a positive divergence dynamic pressure. The Southwell plot in Figure 25 shows this dynamic pressure to be .1943 psi.

The results are summarized in Figures 26 and 27. The fiber orientation of the two outer plies is plotted on the horizontal axis and the predicted divergence dynamic pressure is plotted on the vertical axis. Figure 26 shows these points plotted for the 15° forward swept configuration. The cases with the 110° and 120° plate are divergence free. Fiber orientations outside of the 90° and 140° range seemed to be ineffective in increasing the divergence dynamic pressure. Figure 27 shows the same plot but for the 30°, 45°, and the 60° forward swept cases. For each sweep case, maximum divergence dynamic pressure is found for plates with fibers swept between 0° and 30° forward of the spanwise reference axis. As the wing is swept forward to 45°, the maximum divergence dynamic pressure decreases. This implies that at 45° forward sweep, more bend/twist coupling is required in the structure to regain the same divergence boundary which is characteristic of a 30° or 15° forward swept wing. Maximum divergence dynamic pressure for the 60° forward swept configuration is slightly higher than for the 45° forward swept configuration. In addition, this peak is located along the curve where fibers are nearly spanwise. This would indicate that bending stiffness becomes a predominate factor over bend/twist coupling for highly forward swept wings.

Figures 28, 29, and 30 present the experimental results for q_d as a function of sweep for all configurations. Minimum values of q_d for each plate configuration varied. For cases with the 20° plate, minimun q_d occurred near 50° sweep. With the 80° plate, minimum q_d occurred near 30° sweep. The 100° plate cases showed a shift of minimum q_d to 45° sweep. The 110° and 120° plates have a shift in the minimum q_d beyond 60° sweep. The 140° and 160° plates have a minimum q_d near 45° sweep.

Two factors plagued the numerical analysis of the models. The first factor is found in the plate construction. The construction process had to be completed rapidly to meet wind tunnel scheduling

48
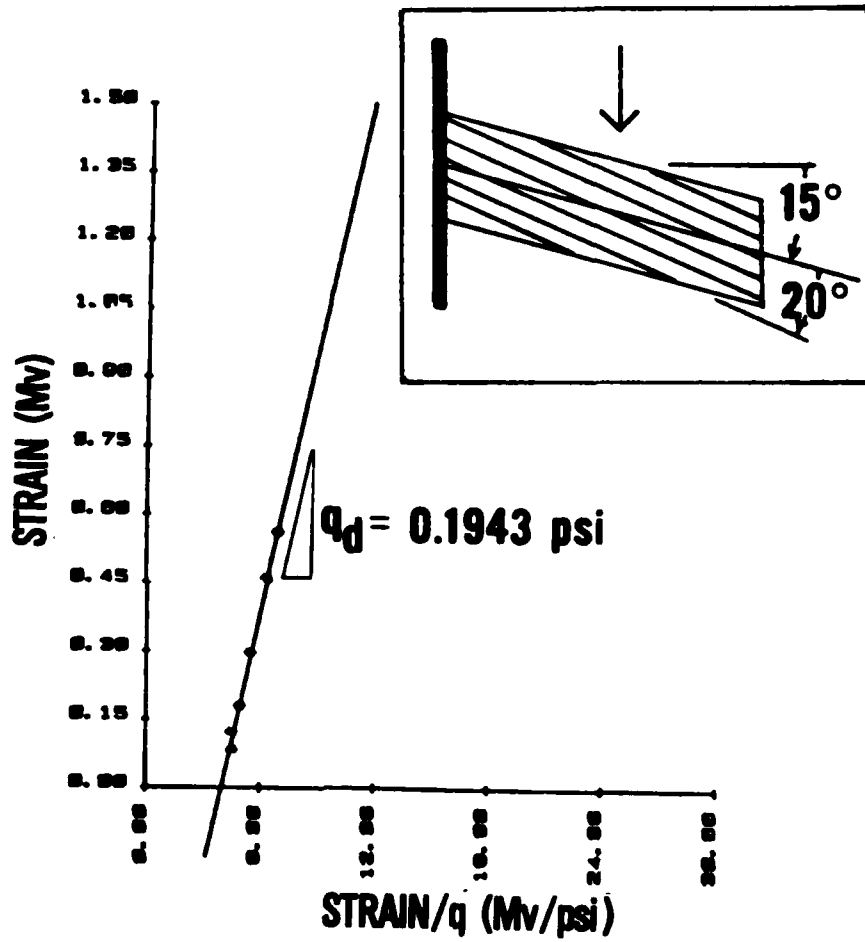
Figure 25.   Southwell Plot for the 15º Aft Swept Configuration with a
70º Plate

49
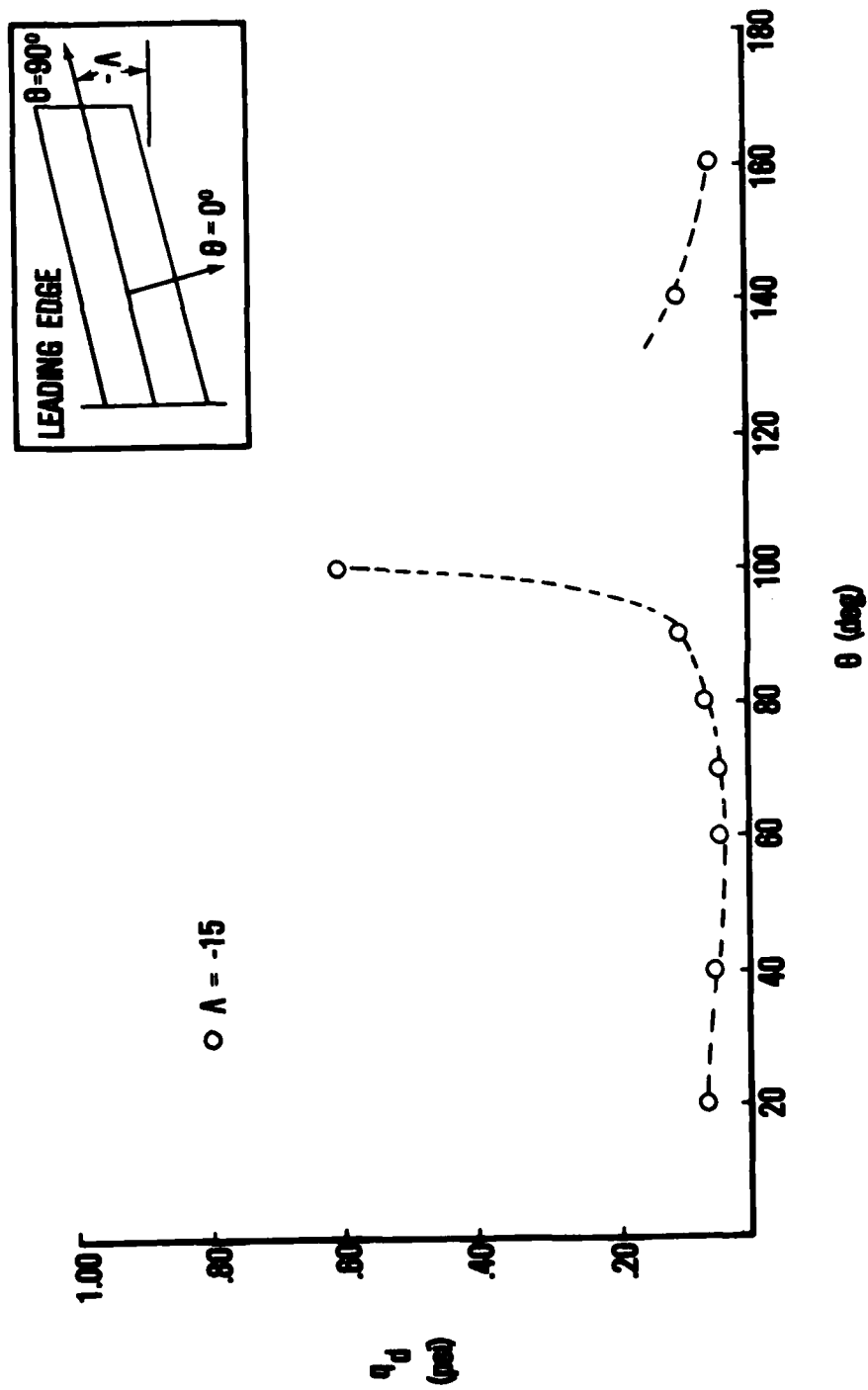
Figure 26. Test Results; q_d as a Function of Fiber Orientation for Λ = -15⁰
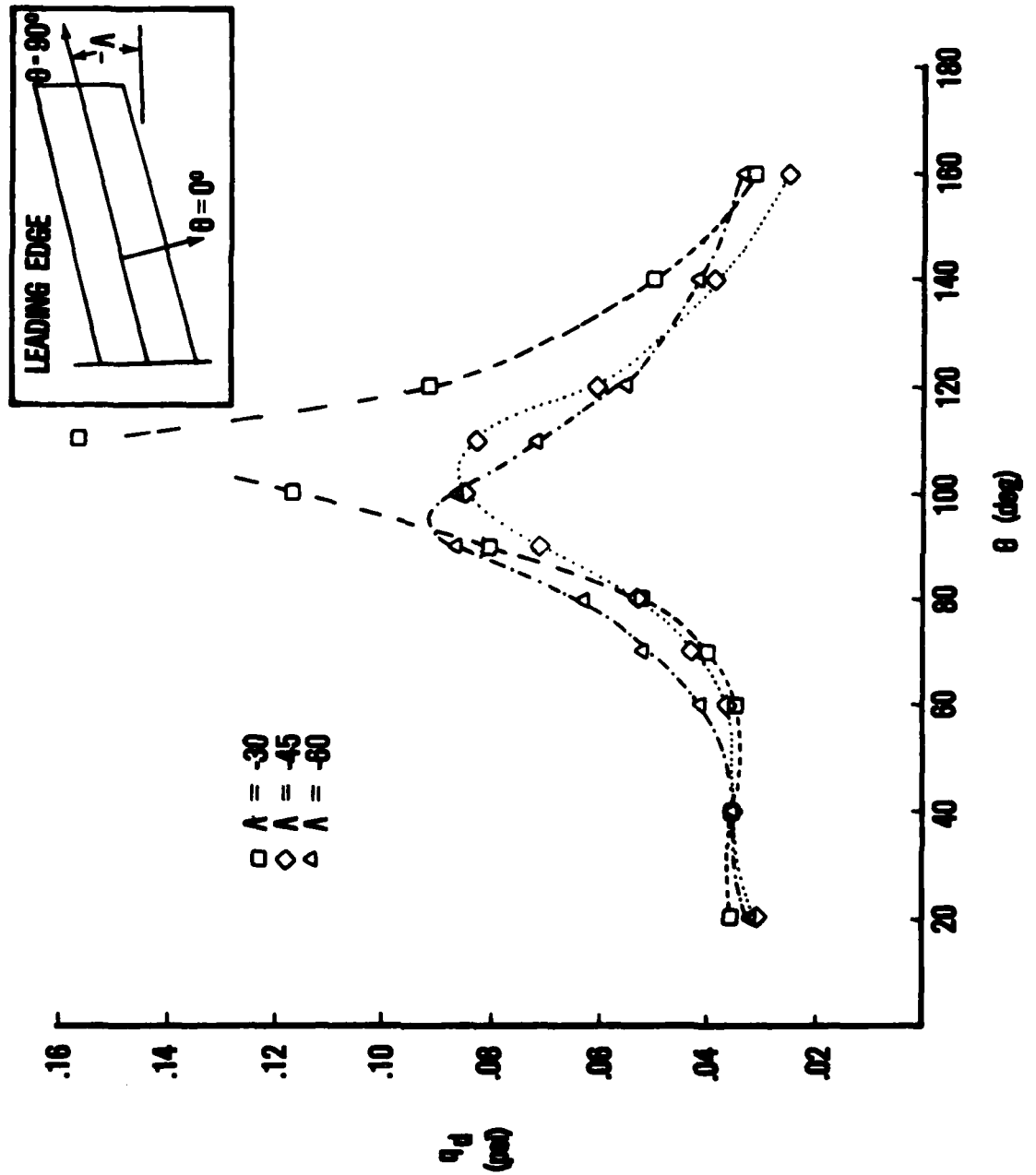
Figure 27. Test Results; q_d as a Function of Fiber Orientation for $\Lambda = -30°$, $-45°$, and $-60°$
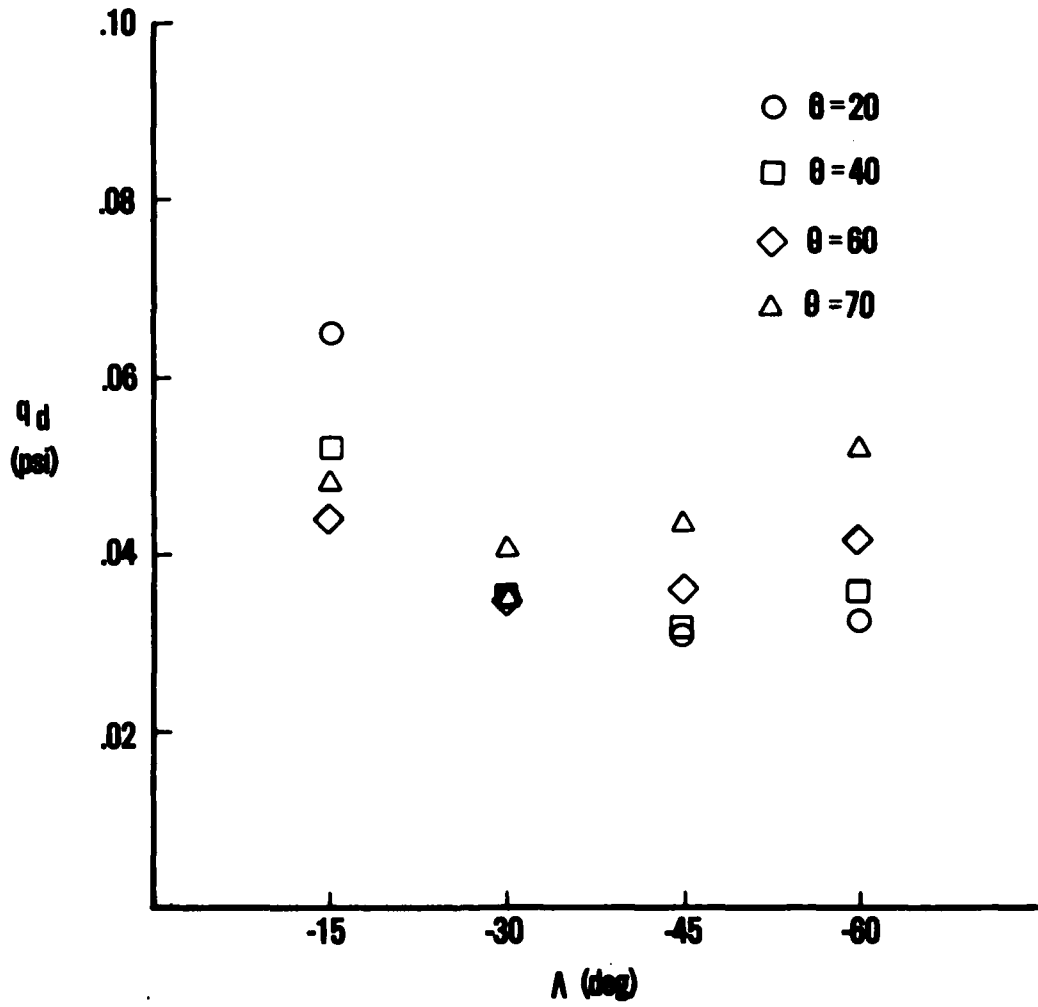
Figure 28. Experimental Results; q_d as a Function of Sweep, $\theta = 20^o$, 40°, 60°, and 70°
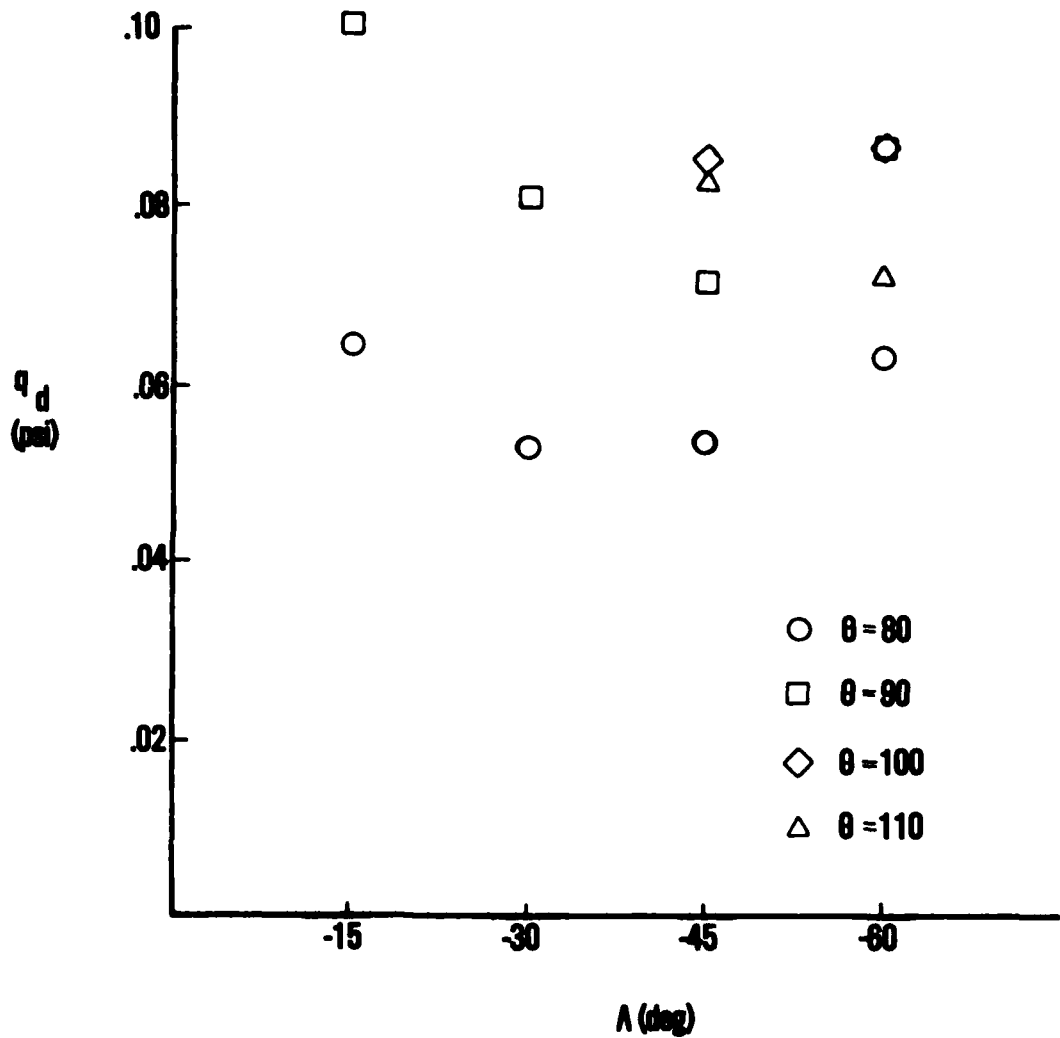
Figure 29. Experimental Results; q_d as a Function of Sweep, θ = 80°, 90°, 100°, and 110°

53
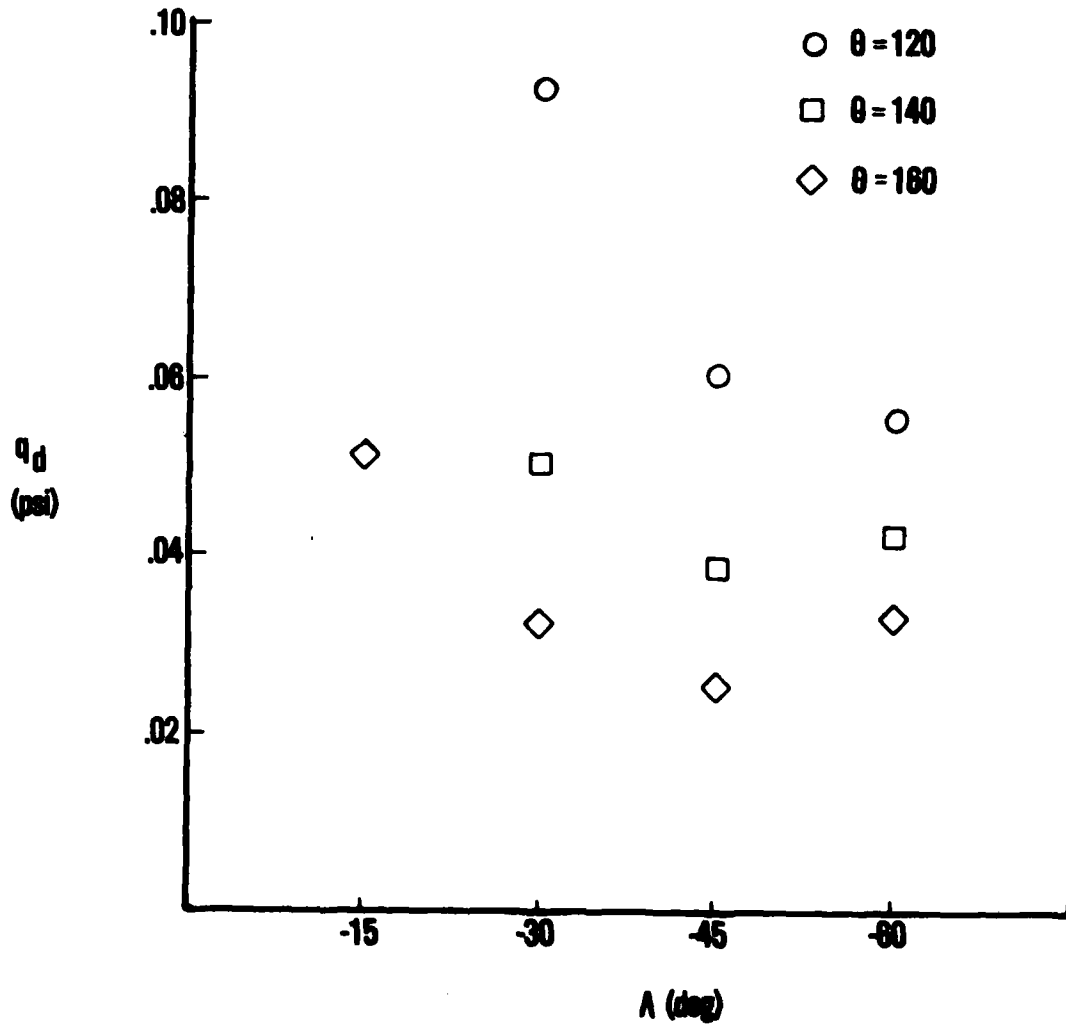
Figure 30. Experimental Results; q_d as a Function of Sweep, $\theta = 120^\circ$, 140°, and 160°

deadlines. New techniques of laminate construction were used at the expense of thickness tolerance. As a result, it was not expected that bending, torsional and bend/twist coupling parameters would be faithfully calculated for all six plates. The bending and torsional stiffness of the wing with the 90° plate were experimentally derived. Divergence dynamic pressures based on the experimental stiffness were calculated using an altered version of Program Three (see Section III) and the results are shown in Figure 31. In this figure, wing sweep is plotted on the horizontal axis and divergence dynamic pressure is plotted on the vertical axis. The four plotted points are divergence dynamic pressures experimentally projected by the Southwell method. The lack of excellent correlation leads one to assume another factor which was present in the wind tunnel experiment and not incorporated into the numerical analysis. An explanation follows:

In order to allow the wing to flex within the fairing, the slot through which the wing protruded was cut oversized. With the wind tunnel control room sealed from the outside, control room pressure should remain equal to the test section static pressure. When air flow is present in the tunnel, pressure in the test section and control room drop. In reality, outside air seeps into the control room. The pressure gradient between the control room and the test section causes leakage into the test section. One place in which air is pulled into the test section is the fairing slot where the wing protrudes into the tunnel. The result is that blowing over the wing root is present in the vertical direction. This blowing was witnessed when the tufts were used for flow visualization. The size of the hole which changes with changing angle-of-attack seems to have an effect on the airflow thus changing the divergence speed. This was brought to light when three Southwell plots were made for the same wing configuration at three root angles of attack. By linear theory, there should be no change in predicted divergence speeds. However, root angles-of-attack of one, two, and three degrees yielded predicted divergence dynamic pressures of .0714, .0715, and .0609 psi, respectively. It was noted that the change in angle caused a change in fairing gap opening. Four cases were run with the 90° plate in order to demonstrate the extent to which the gap

55
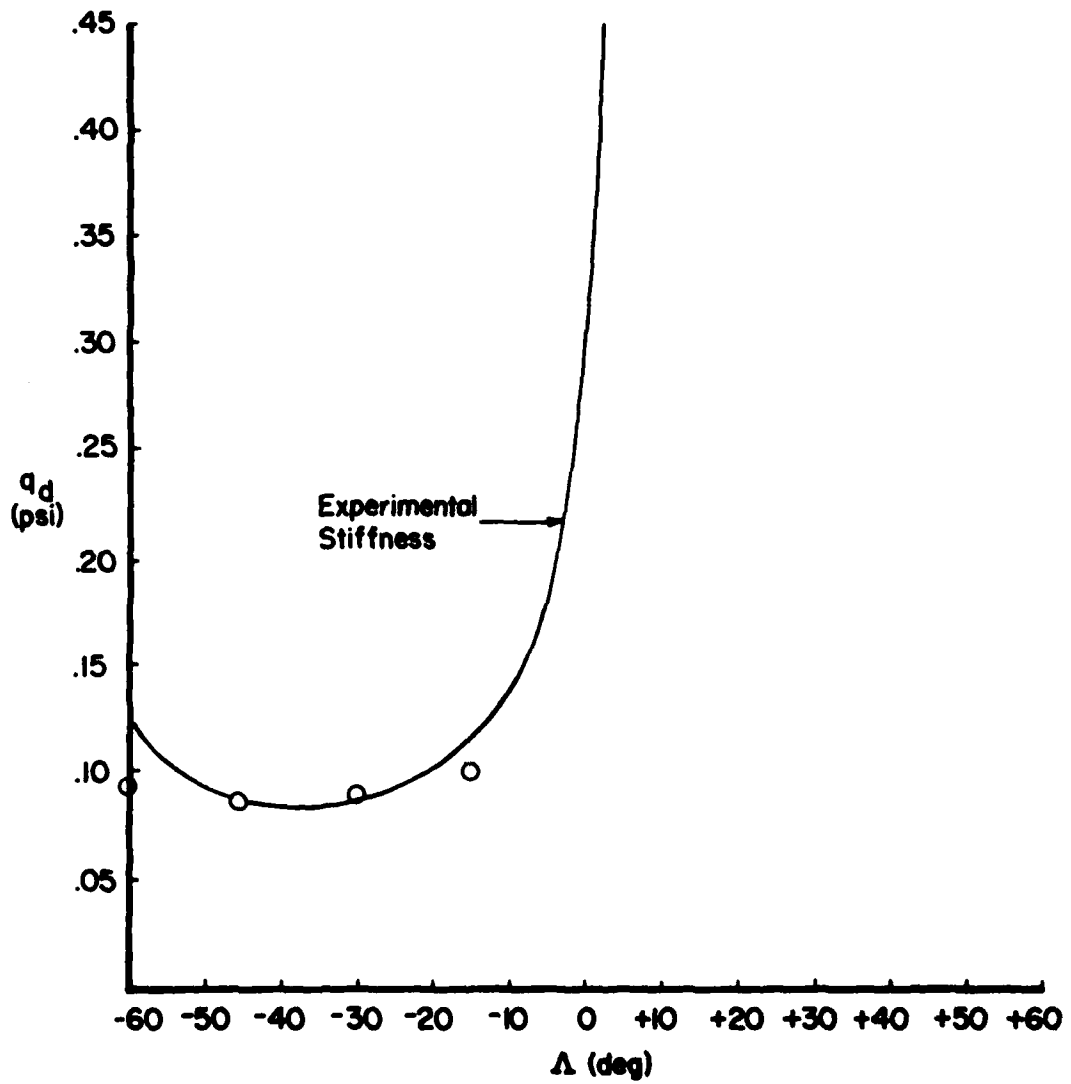
Figure 31. Correlation of Results and Numerical Calculations without Interference Effects

size influenced the results. Cases 72 and 73 are at 30° sweep with normal opening and closed opening. Predicted q_d dropped from 0.08 psi to .0768 psi. Cases 74 and 75 are at 45° sweep with closed and normal opening. Predicted q_d rose from .0691 psi to .0708 psi. Cases 72 and 75 have openings of size nominally equal to all other test runs. Cases 73 and 74 have only a very small opening which allows only for the small amount of vertical flow near the root.

As a means of verifying theoretical trends, Figure 32 was drawn. The solid lines represent the preliminary CWING analysis at various sweep angles and without stiffness or aerodynamic correction. Experimental points are plotted for the -15°, -30°, -45°, and -60° sweep cases. While results are not expected to match the CWING analysis, the trends correlate very well. Again, one can see that for moderately forward swept configurations (-45° or less), divergence is best controlled with fibers swept forward of the spanwise reference axis. For highly forward swept configurations, bending stiffness becomes the predominate factor in controlling wing divergence.

At the end of the test program, some of the plates were tested for divergence without the aerodynamic shell attached. This would eliminate the shell stiffness contribution and shell aerodynamic behavior from consideration in determining the main factors which would create the present discrepancy between the CWING preliminary analysis and experimental results. The results of these tests are also given in Appendix A and shown in Figure 33. Each line represents the CWING preliminary analysis based on an aerodynamic model of the same dimensions as the 24 ply plate uncorrected for thickness. One can see that experimental results lay consistently below the CWING analysis. If the analysis had been corrected for stiffness, the difference between experiment and analysis would have been made greater. One may assume that aerodynamic conditions at the root contributed to some of the discrepancy. The greatest discrepancy was formed at -60° sweep in which case the root condition is most distorted.
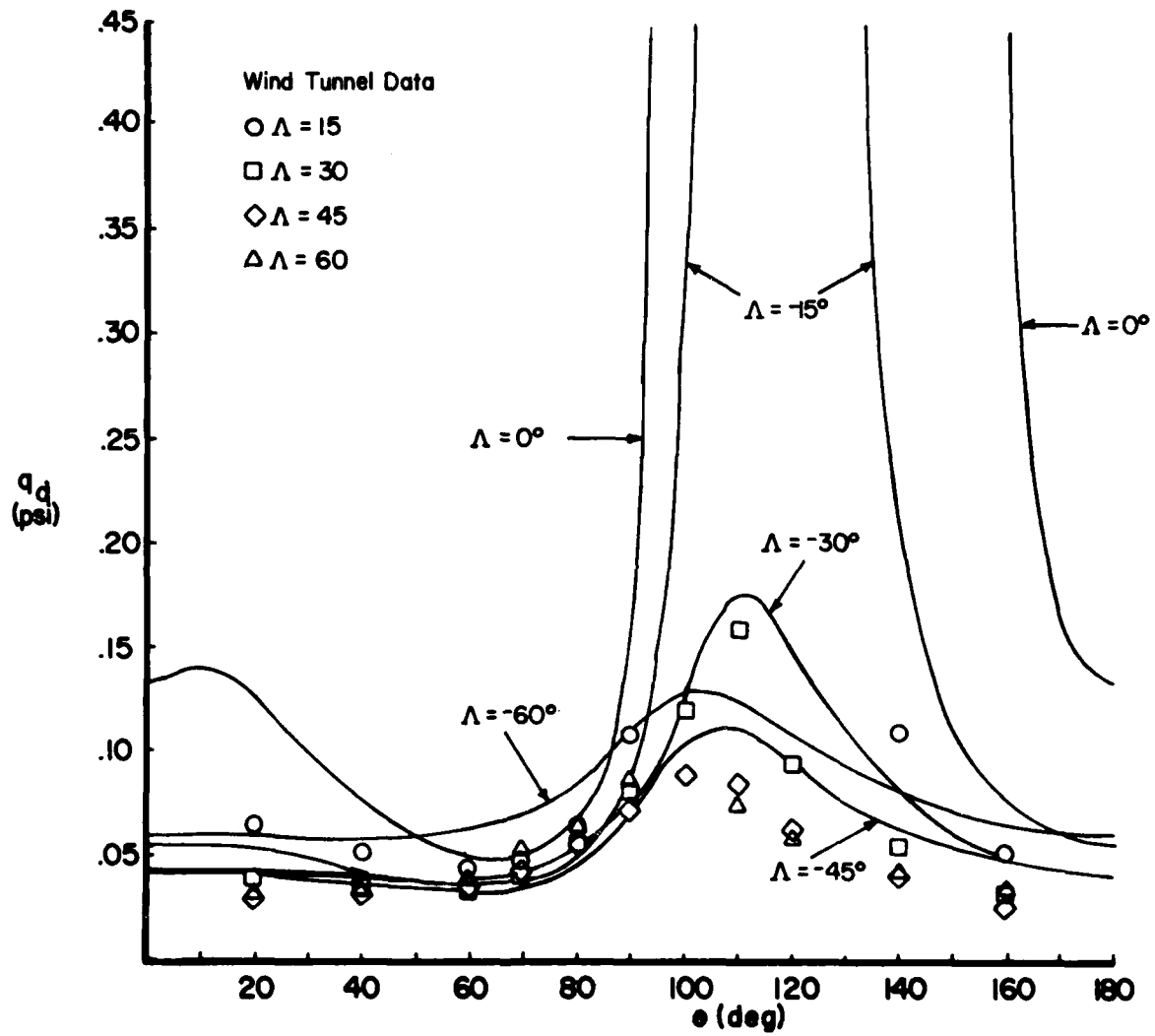
Figure 32. Design Calculations and Experimental Results; q_d as a Function of Fiber Orientation
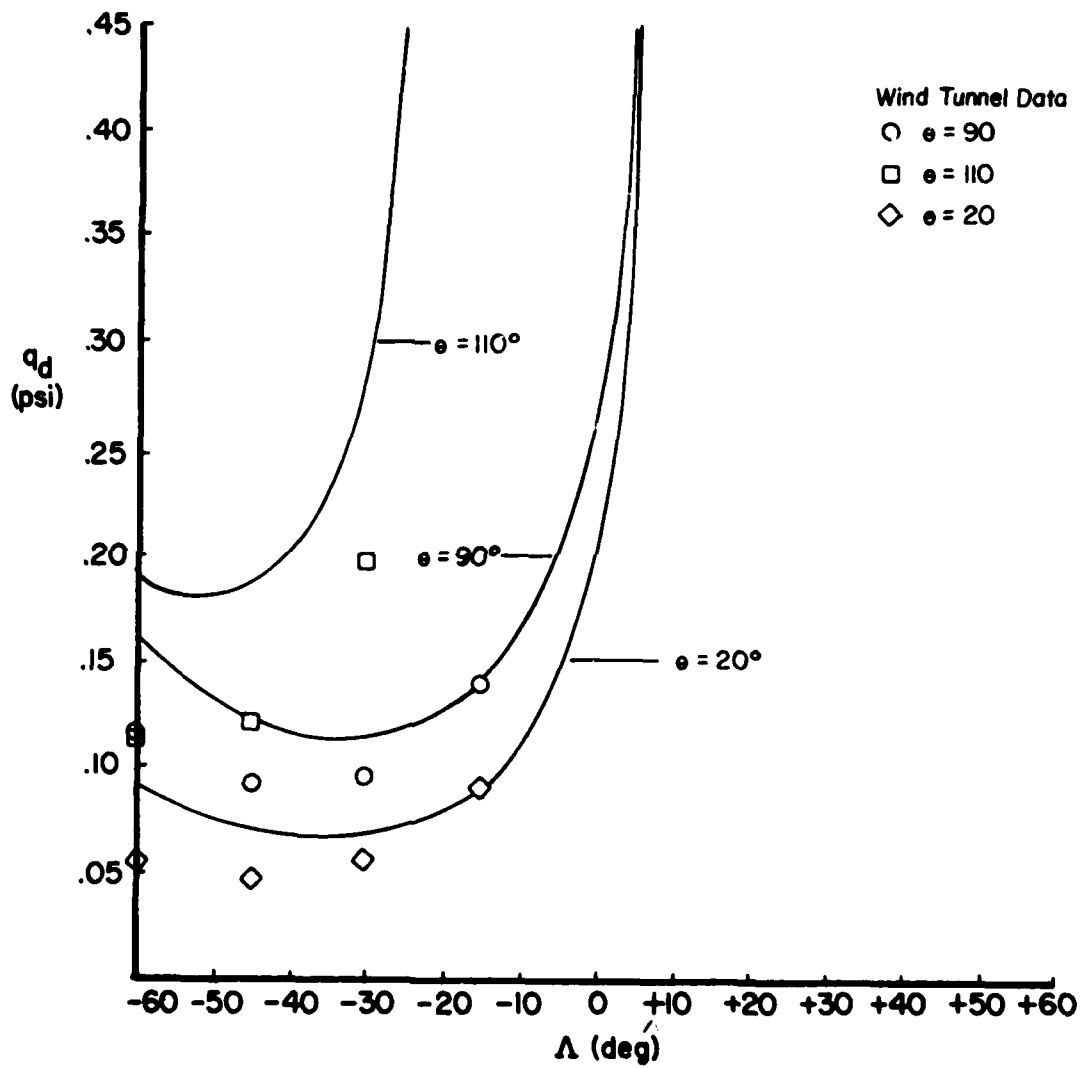
Figure 33. Plate Alone Results Compared to Design Calculations; q_d as a Function of Sweep

As a final means of correlating results, a divergence hard point was obtained after a Southwell projection was made. The 30° forward swept configuration with a 20° plate was chosen for this test. The divergence hard point was approached by unloading the wing as the dynamic pressure increased. The dynamic pressure at which the clamped wing diverged was .0394 psi. The Southwell technique projected a divergence dynamic pressure of .0379 psi, a difference of 4%.

An accidental overload was encountered during a Southwell test on Case 7 with the 90° plate at -60° sweep. Throughout the test the wing was lightly loaded at a q of .0650 psi. At a q of .0660 psi, the wing overloaded. The overloading was apparent as the wing suddenly deflected to one side until the wing root hit the slot in the fairing. Apparently, the root angle-of-attack was very small and, therefore there was little warning that the wing was at or near the divergence speed. The q_d prediction by the Southwell method for Case 7 was .0628 psi, however, the last data point was taken as the tunnel was being shut down. The repeated test, Case 8, predicted a divergence q of .0664 psi by Southwell's method. Due to this danger of overloading the wing at small root angles-of-attack, the experimental procedure was changed to ensure a minimum of one degree angle-of-attack was present.

SECTION VII

CONCLUSIONS

It has been shown that divergence of a wing structure can be effectively controlled by varying fiber orientation of selected plies. By the introduction of bend/twist coupling, wing washin properties can be neutralized and the divergence problem avoided.

Maximum divergence speeds are found in wings with fibers swept 0 to 30 degrees forward of the reference axis. Fibers in this direction cause washin of the wing to be minimized. The converse is true for fibers which are swept rearward since the wing washes in and divergence speed drops. Highly forward swept wings need less bend/twist coupling and more bending stiffness to control divergence. Therefore, these configurations need fibers which are swept only slightly forward of the reference axis. Moderately forward swept wings need more bend twist coupling to maintain high divergence speeds. Therefore, fibers must be swept further forward than required on highly forward swept configurations.

Divergence speed decreases as the wing sweeps forward from 0° until a minimum speed is encountered. In all cases, the minimum divergence speed is encountered at forward sweeps of 30 degrees or more.

The construction of this aeroelastic wind tunnel model was greatly complicated by the incorporation of the aerodynamic shell. In addition, the method of connecting the shell to the plate produced a stiffness factor which was difficult to analyze. The wind tunnel tests with no sleeve resulted in Southwell plots with no more anomalies than tests with the sleeve attached. Therefore, it is the opinion of this author that the use of the aerodynamic shell was an unnecessary complication in these divergence tests. The author would also like to suggest the incorporation of aerodynamic interference effects in any divergence analysis.

The divergence phenomenon is defined for a clamped wing. For a free flying airplane, this clamped condition is not correct and a dynamic analysis is required to define a stability boundary. For this reason, it is important to view the results of this experiment as a benchmark of static aeroelastic stability. This benchmark relates only the aerodynamic load distribution and the ability of the restrained wing to elastically compensate for this load.

REFERENCES

1. N. J. Krone, Jr., "Divergence Elimination with Advanced Composites", AIAA Paper #75-1009, 1975.

2. M. R. Robinson and D. A., Robinson, "Forward Swept Wing Designs: A High Payoff Through Technology Integration", AIAA Paper #80-1884, 1980.

3. N. J. Krone, Jr., "Forward Swept Wing Demonstrator", AIAA Paper #80-1882, 1980.

4. L. S. Jones, US Bombers B1-B70, Aero Publishers, Los Angeles, CA., 1962.

5. F. W. Diederich and B. Budiansky, Divergence of Swept Wings, NACA TN 1680, 1948.

6. R. L. Bisplinghoff, H. Ashley, and R. L. Halfman, Aeroelasticity, Addison-Wesley Publishing Co., Reading, MA 1955.

7. L. A. Schmit, "The Structural Synthesis Concept and its Potential Role in Design with Composites", Mechanics of Composite Materials Proceedings of the Fifth Symposium on Naval Structural Mechanics (1967) Pergamon Press, 1970.

8. L. A. McCullers and R. W. Lynch, "Composite Wing Design for Aeroelastic Tailoring Requirements", Presented at the Air Force Conference on Fibrous Composites in Flight Vehicle Design in Dayton, Ohio, 26-28 Sep 72.

9. R. W. Lynch and W. A. Rogers, "Aeroelastic Tailoring of Composite Materials to Improve Performance", Presented at the AIAA/ASME/SAE 17th Structures, Structural Dynamics and Materials Conference, Valley Forge, PA, 5-7 May 76.

10. J. W. Ellis, S. K. Dobbs, and G. D. Miller, Structural Design and Wind Tunnel Testing of a Forward Swept Fighter Wing, AFWAL-TR-80-3073, April 1980.

11. K. Wilkinson and F. Rauch, Predicted and Measured Divergence Speeds of an Advanced Composite Forward Swept Wing Model", AFWAL-TR-80-3059, July 1980.

12. V. C. Sherrer, T. J. Hertz, and M. H. Shirk, "A Wind Tunnel Demonstration of the Principle of Aeroelastic Tailoring Applied to Forward Swept Wings", AIAA Paper #80-0796 presented at 21st SDM Conference

13. R. H. Ricketts and R. V. Doggett, "Wind Tunnel Experiments on Divergence of Forward Swept Wings," NASA TP 1685, August 1980.

14. T. A. Weisshaar, "Divergence of Forward Swept Composite Wings", AIAA Journal of Aircraft, Vol. 17, No. 6, pp. 442-448, June 1980.

REFERENCES (Cont'd)

15. A. H. Flax, "The Influence of Structural Deformation on Airplane Characteristics", Journal of Aeronautical Science, Vol. 12, No. 1, Jan 1945, pp. 94-102.

16. R. V. Southwell, "On the Analysis of Experimental Observations in Problems of Elastic Stability", Proceedings of the Royal Society (London), Ser. A, Vol. 135, April 1, 1932, pp. 601-616.

17. M. Blair, "Experimental Measurement of Wing Divergence Velocity", Presented at the AIAA Southeast Region Student Conference, April 1978.

18. M. Blair, "Experimental Measurement of Swept Forward Wing Divergence Velocity", Presented at the AIAA Southeast Region Student Conference, April 1979.

19. T. A. Weisshaar, The Influence of Aeroelasticity on Swept Composite Wings, AFWAL-TR-80-3137, Vol. 1, Nov 1980.

20. J. Alexander, "Foam Wings", R/C Modeler Corp., 1971.

APPENDIX

DATA SYNOPSIS

The data presented in this appendix was chosen from the test results to be representative of all the wind tunnel tests. There are a total of eight columns. The first two columns represent fiber angle and wing sweep, both measured in degrees. The next three columns, headed SHELL ATTACHED, represent the cases for which the aerodynamic shell was attached. The last three columns, headed PLATE ALONE, represent the cases for which the aerodynamic shell was removed. Under the heading, SHELL ATTACHED, are headings which denote results from the CWING analysis, the Southwell plot case number, and results from the Southwell tests. Under the heading, PLATE ALONE, are headings which again denote results from the CWING analysis, but for no aerodynamic shell, the Southwell plot case number and results from the Southwell tests on plates with no aerodynamic shell.

		SHELL ATTACHED			PLATE ALONE		
FIBER ANGLE	WING SWEEP	q_d(psi) CWING	CASE NUMBER	q_d(psi) TEST	q_d(psi) CWING	CASE NUMBER	q_d(psi) TEST
Alum	-15	.0963	4	.0854			
Alum	-30	.0642	1	.0540			
Alum	-45	.0614	2	.0417			
Alum	-60	.0793	3	.0468			
20	-15	.0534	54	.0650	.0906	84	.0913
20	-30	.0408	79	.0357	.0689	83	.0553
20	-45	.0423	80	.0306	.0711	81	.0487
20	-60	.0597	57	.0322	.0911	82	.0531
40	-15	.0425	45	.0519			
40	-30	.0359	46	.0356			
40	-45	.0393	47	.0318			
40	-60	.0578	48	.0355			
60	-15	.0362	19	.0440			
60	-30	.0337	20	.0349			
60	-45	.0393	21	.0365			
60	-60	.0608	22	.0415			
70	+15	.101	40	.1943			
70	-15	.0378	36	.0477			
70	-30	.0362	37	.0406			
70	-45	.0431	38	.0434			
70	-60	.0678	39	.0522			

FIBER ANGLE	WING SWEEP	SHELL ATTACHED			PLATE ALONE		
		q_d(psi) CWING	CASE NUMBER	q_d(psi) TEST	q_d(psi) CWING	CASE NUMBER	q_d(psi) TEST
80	-15	.0478	27	.0641			
80	-30	.0451	28	.0528			
80	-45	.0533	29	.0533			
80	-60	.0832	30	.0631			
90	-15	.0852	10	.1006	.141	85	.1308
90	-30	.0696	63	.0809	.115	86	.0979
90	-45	.0749	66	.0714	.124	88	.0935
90	-60	.1090	70	.0866	.164	89	.1180
100	-15	.321	26	.6095			
100	-30	.124	23	.1174			
100	-45	.104	24	.0851			
100	-60	.129	25	.0861			
110	-15	-1.35	31	-.3865			
110	-30	.176	33	.1571	.287	91	.1926
110	-45	.111	34	.0830	.186	92	.1283
110	-60	.124	35	.0720	.190	93	.1159
120	-15	-.962	18	-.4912			
120	-30	.151	15	.0927			
120	-45	.0959	16	.0607			
120	-60	.107	17	.0557			

FIBER ANGLE	WING SWEEP	SHELL ATTACHED			PLATE ALONE		
		q_d(psi) CWING	CASE NUMBER	q_d(psi) TEST	q_d(psi) CWING	CASE NUMBER	q_d(psi) TEST
140	-15	.215	41	.1071			
140	-30	.0788	42	.0503			
140	-45	.0645	43	.0388			
140	-60	.0796	44	.0421			
160	-15	.0758	49	.0515			
160	-30	.0499	50	.0324			
160	-45	.0482	51	.0253			
160	-60	.0651	52	.0331			